Tetra-Armed Oligo(Phenylenevinylene)-Based Covalent Organic Frameworks for Enhanced Photocatalytic Hydrogen Evolution

Jinwei Yuan,[a] Xingjiang Yu,[a] Wenbo Dong,[a] Zhiying Qin,[a] Longyu Li[a,*]

a. College of Polymer Science and Engineering, State Key Laboratory of Advanced Polymer Materials, Sichuan University, Chengdu, 610065, Sichuan

E-mail: longyu88@scu.edu.cn

Table of Contents

Section S1. General materials and methods

Materials

If not stated otherwise, all reagents were purchased from commercial sources and used without any further purification. 1,2,4,5-Tetrakis(bromomethyl)benzene (≥ 97%), triethyl phosphite (≥ 98%), p-phthalaldehyde (≥ 98%), p-phenylenediamine (≥ 99%), tetrahydrofuran (≥ 99.5%), potassium tert butoxide (≥ 99%), p-nitrobenzaldehyde(≥ 99%) mesitylene (≥ 99%), dioxane (≥ 99.5%), o-dichlorobenzene (≥ 98%), n-butanol (≥ 99%), methanol (≥ 99.5%), ethanol (≥ 99.7%), acetone (≥ 99.5%), sodium hydroxide (≥ 99.5%), sodium sulfide hydrochloric acid (36%-38%), sodium sulphide nonahydrate(≥99%) dichloromethane (≥ 99.5%), acetic acid (≥ 99%), sodium sulfate anhydrous (≥ 99%), potassium chloride (≥ 99%), triethanolamine (≥ 99%), ascorbic acid (≥ 99%) and sodium chloride (≥ 99.5%) pyridine (≥ 99.5%) dimethyl sulfoxide (≥ 99.5%) benzoic acid (≥ 99%),benzonitrile (≥ 99%),aniline(≥ 99%) were purchased from Adamas-beta. Nafion D-520 dispersion was purchased from Alfa Aesar.

Characterization

^{1}H NMR spectra were measured on a Bruker AVANCE III HD spectrometer operating at resonance frequencies of 400 MHz and are reported in ppm using solvent as an internal standard ($CDCl_3$ at 7.26 ppm for ^{1}H). Fourier transform infrared (FT-IR) spectra were recorded on a Nicolet NEXUS 670 spectrometer. The IR of the samples were collected with a universal diamond ATR (attenuated total reflection) in the 650 ~ 4000 cm^{-1} region. Powder X-ray diffraction (PXRD) patterns were obtained on a MiniFlex 600 X-ray diffraction system (Cu, K_{a1} = 1.540598, K_{a2} = 1.544426, from 2° to 30°, step size = 0.01°) with focused radiation at 40 kV and 15 mA. Thermogravimetric analysis (TGA) from 30-800 ℃ was carried out on a METTLER TOLEDO TGA2 in a nitrogen atmosphere using a 10 ℃/min ramp without equilibration delay. The scanning electron microscope (SEM) was performed on a Thermo Scientific Helios 5 CX operating at an accelerating voltage ranging from 0.2 to 30 kV. Transmission Electron Microscope (TEM) was performed on a Thermo Scientific Talos F200X operating at a voltage 40 kV. X-ray photoelectron spectroscopy (XPS) was performed on Thermo Scientific K-Alpha.COFs were activated using supercritical CO_2 with SCD-350M, SCD-380A (Shianjia Technology). The surface areas and pore investigated by nitrogen adsorption and desorption at 77 K using iPore400, iPore600 (PhysiChem Instruments Lid.). The pore-size distribution curves were obtained from the adsorption branches using quenched solid density functional theory (QSDFT). UV-visible absorption spectra of as-obtained materials were measured on a Shimadzu UV-2700 UV-vis spectrometer by measuring the reflectance

of powders in the solid state. The scan was arranged from 200 to 800 nm with the scan rate of medium. Photoluminescence (PL) spectroscopy was recorded via the Fluorolog-3 spectrofluorometer (Horiba JobinYvon) at room temperature. Electrospray Ionization mass spectrum (ESI-MS) were tested by Thermo Scientific Orbitrap Exploris 120. Elemental analysis (EA) was conducted on an elementar vario EL cube.

Section S2. Synthetic procedures

Synthesis of 1,2,4,5-Tetrakis(diethyl methylphosphonate)benzene

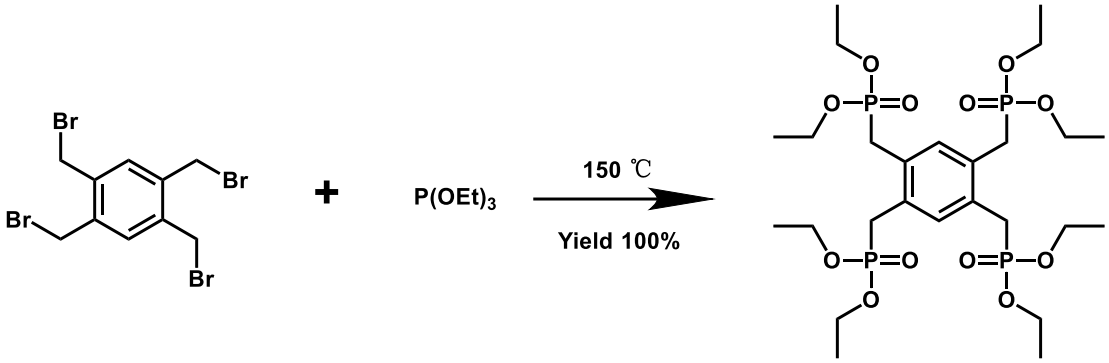

Figure S1. Synthetic routes of 1,2,4,5-tetrakis(diethyl methylphosphonate)benzene.

To a 25 mL single-neck round-bottom flask equipped with a condenser and maintained under a nitrogen atmosphere were added 1,2,4,5-tetrakis(bromomethyl)benzene (0.500 g, 1.11 mmol) and triethyl phosphite (5.0 mL, 29.8 mmol). The reaction mixture was heated at 150 °C with stirring for 4 h, then allowed to cool to room temperature. Excess triethyl phosphite was removed under reduced pressure, and the residue was dried under high vacuum until no condensate was visible in the condenser head, affording the product as a yellow oil.

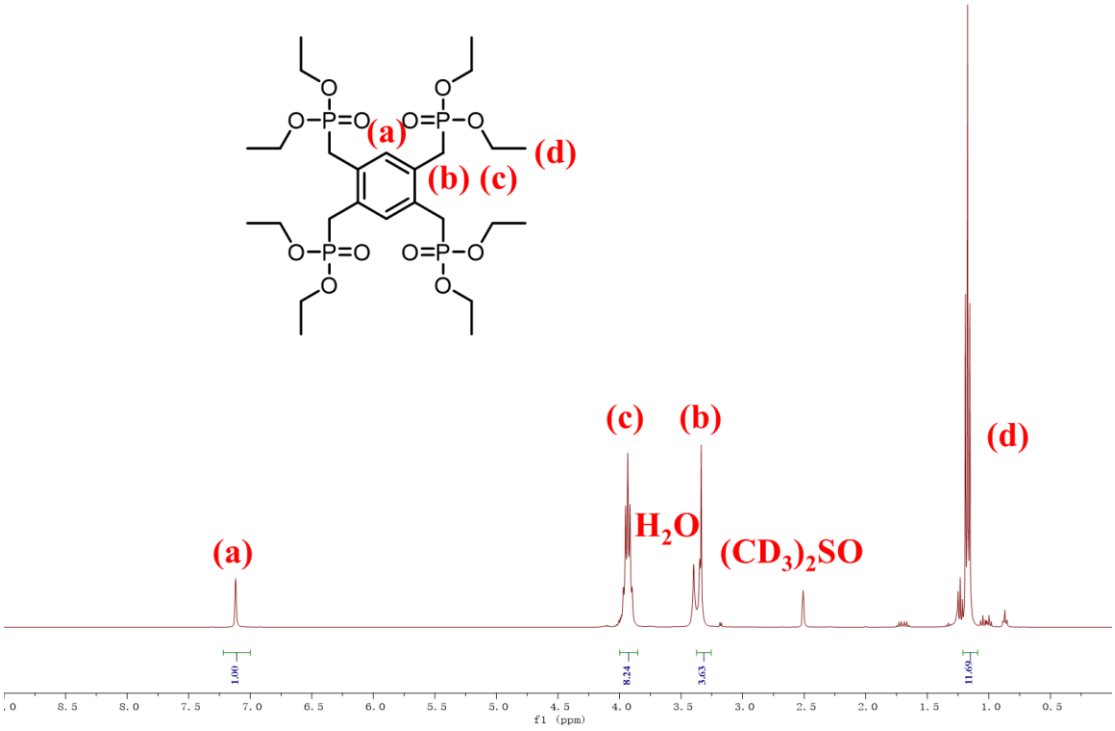

Figure S2. ^{1}H-NMR spectrum of 1,2,4,5-tetrakis(diethyl methylphosphonate)benzene.

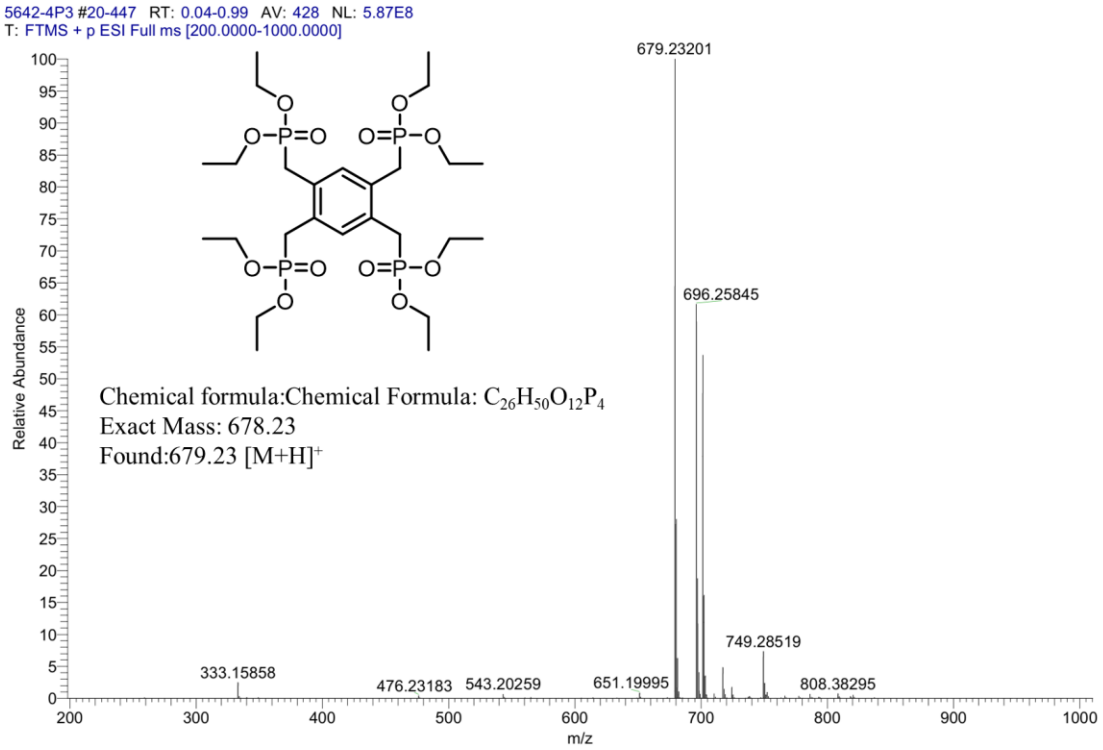

Figure S3. ESI mass spectrum of 1,2,4,5-tetrakis(diethyl methylphosphonate)benzene.

Synthesis of 1,2,4,5-Tetrakis(p-formylstyryl)benzene

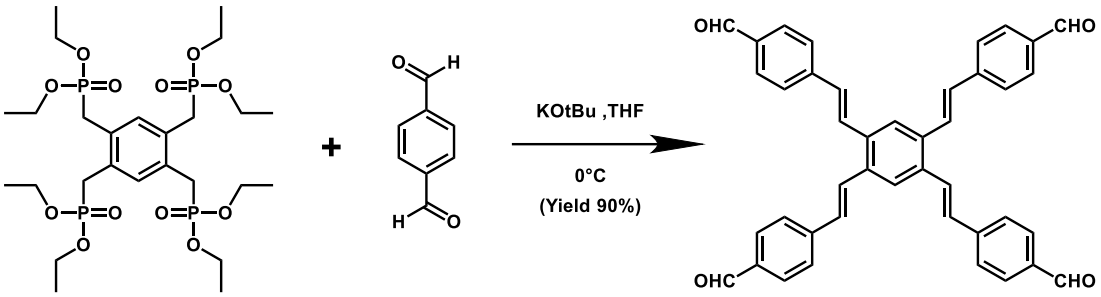

Figure S4. Synthetic routes of 1,2,4,5-tetrakis(p-formylstyryl)benzene.

In a two-neck 250 mL round-bottom flask equipped with a magnetic stir bar and maintained under a nitrogen atmosphere in an ice–water bath were combined 1,2,4,5-tetrakis(diethyl methylphosphonate)benzene (0.754 g, 1.11 mmol), THF (110 mL), and terephthalaldehyde (1.34 g, 9.99 mmol, 9.0 equiv). The mixture was stirred at 0 °C for 20 min, after which potassium tert-butoxide (0.747 g, 6.66 mmol, 6.0 equiv) was added in one portion. The cooling bath was then removed, and the reaction mixture was allowed to warm to room temperature and stirred overnight (~16 h). The reaction was quenched by addition of water (50 mL), and the mixture was acidified to pH ~2 by adding 1 M HCl (10 mL). Stirring was continued for an additional 2 h at room temperature. THF was removed by rotary evaporation to give a suspension. The resulting solid was collected by filtration and washed successively with water (3×) and methanol (3×). The product was dried under vacuum at 40 °C to constant weight to afford an orange solid (0.3245 g, 49% yield based on 1,2,4,5-tetrakis(diethyl methylphosphonate)benzene). ^{1}H NMR (400 MHz, $(CD_3)_2SO$, ppm): δ = 8.21 (s, 2H), 8.01 (s, 4H), 7.50 (s, 4H), 7.94 (d, 8H), 7.96 (d, 8H) ,10.02 (s, 4H). ^{13}C NMR (101 MHz,

DMSO-d6): δ (ppm) 192.91, 143.59, 135.71, 131.12, 130.44, 129.93, 128.89, 128.07, 127.94, 124.78.

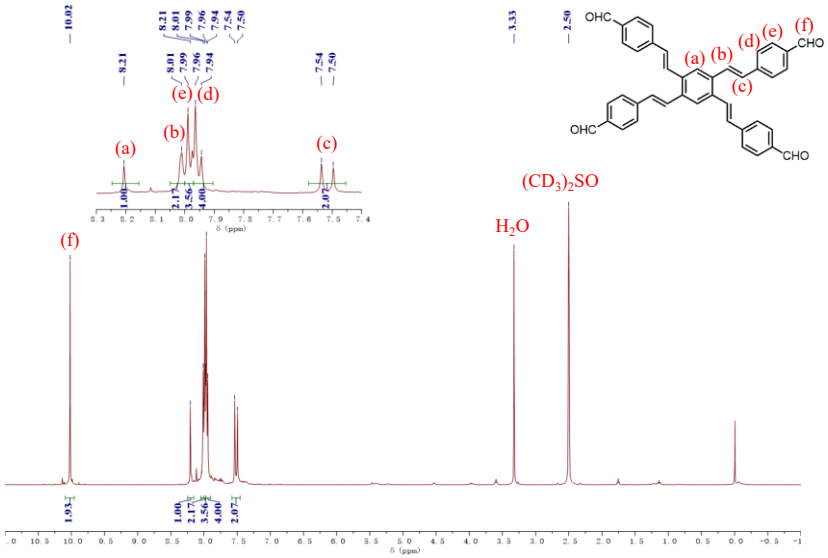

Figure S5. ^{1}H-NMR spectrum of 1,2,4,5-tetrakis(p-formylstyryl)benzene.

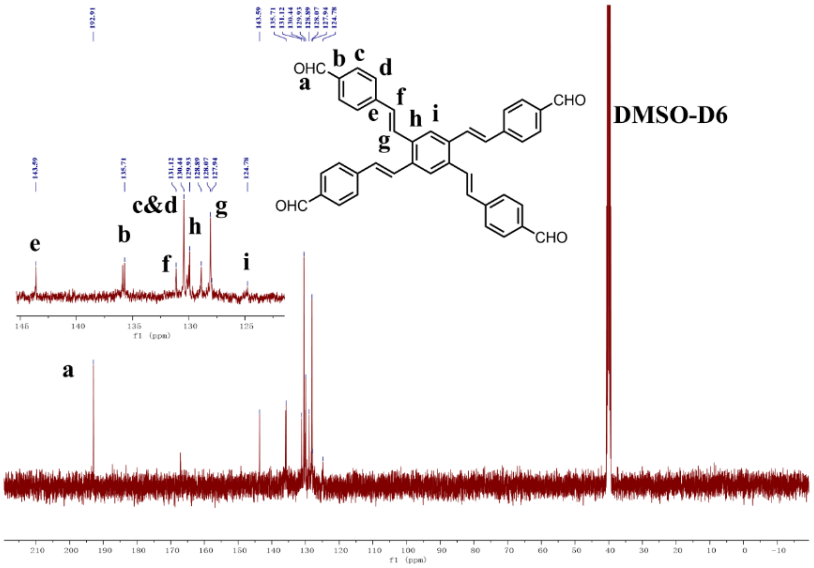

Figure S6. ^{13}C-NMR spectrum of 1,2,4,5-tetrakis(p-formylstyryl)benzene.

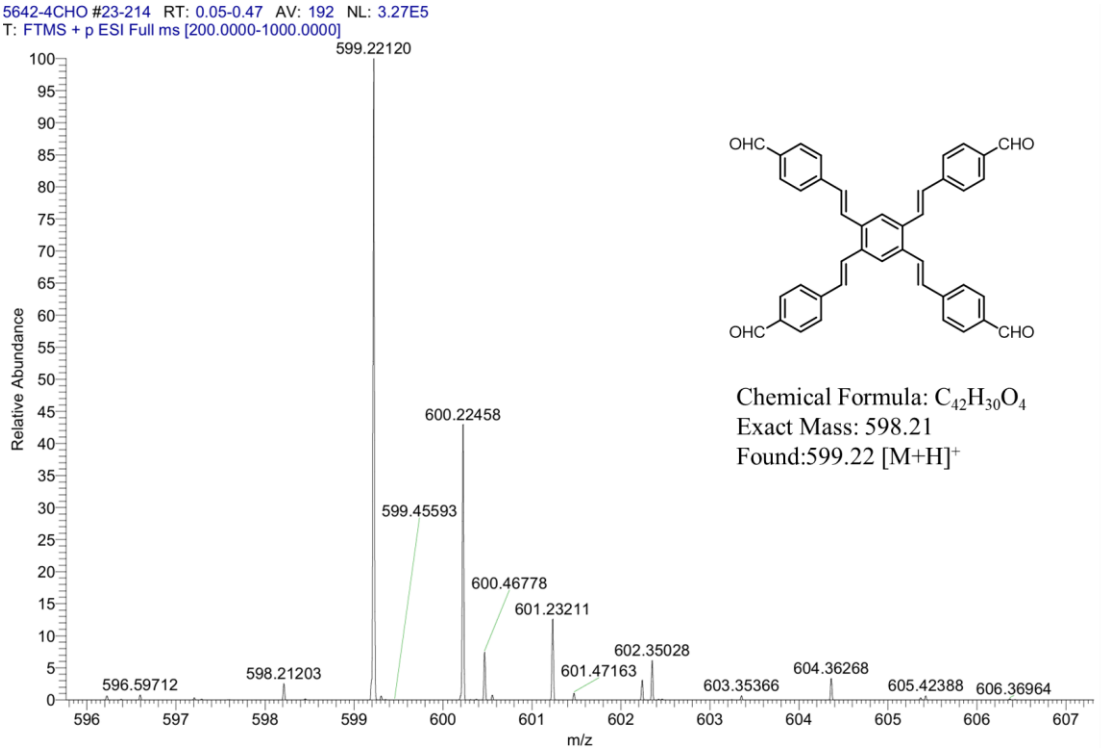

Figure S7. ESI mass spectrum of 1,2,4,5-tetrakis(p-formylstyryl)benzene.

Synthesis of 1,2,4,5-Tetrakis(p-nitrophenylvinyl)benzene

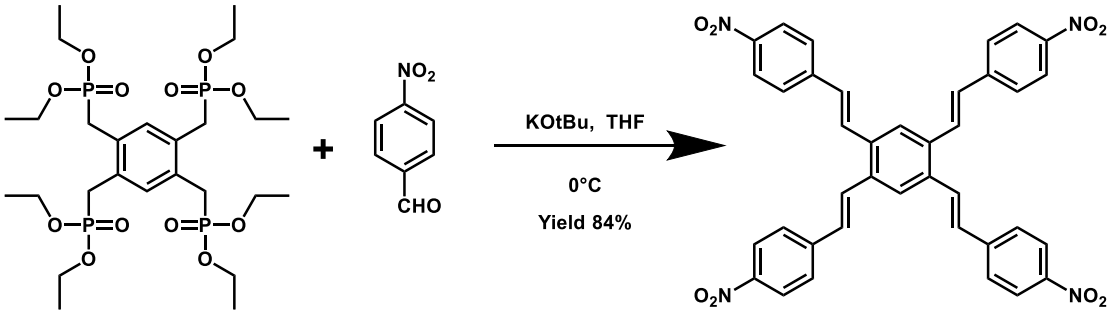

Figure S8. Synthetic routes of 1,2,4,5-tetrakis(p-nitrophenylvinyl)benzene.

In an ice–water bath, a nitrogen-flushed two-neck 250 mL round-bottom flask equipped with a magnetic stir bar was charged with potassium tert-butoxide (1.245 g, 11.1 mmol, 10.0 equiv) dissolved in dry THF (13 mL) to give a pale yellow, clear solution. In a separate vessel, 1,2,4,5-tetrakis(diethoxyphosphinomethyl)benzene (0.754 g, 1.11 mmol) and p-nitrobenzaldehyde (1.511 g, 9.99 mmol, 9.0 equiv) were dissolved in dry

THF (13 mL) with brief bath sonication (~2 min) to afford a homogeneous yellow solution. This reagent solution was transferred to a pressure-equalizing dropping funnel and added dropwise to the vigorously stirred, ice-cooled t-BuOK solution under nitrogen. During the addition the reaction mixture darkened (black–green) and became turbid. After the addition was complete, stirring was maintained in the ice bath for a short period (⩽10 min), then the cooling bath was removed and the mixture was allowed to warm to room temperature and stirred for 24 h. The reaction was quenched by slow addition of water (100 mL); the mixture turned brownish-yellow and heavy precipitation formed. The suspension was acidified to pH 2–3 by addition of 1 M HCl (20 mL), giving an orange-yellow slurry. The solid was collected by filtration and washed successively with water (3 × 100 mL), methanol (3 × 30 mL), and dichloromethane (3 × 30 mL). The product was dried under vacuum to constant mass to yield an orange powder.

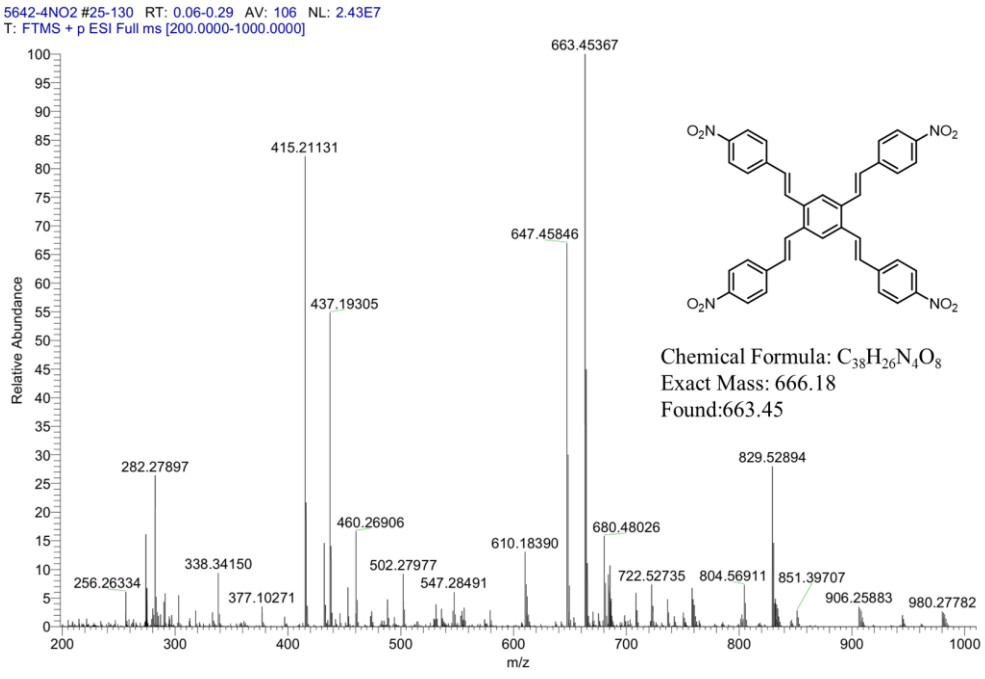

Figure S9. ESI mass spectrum of 1,2,4,5-tetrakis(p-formylstyryl)benzene.

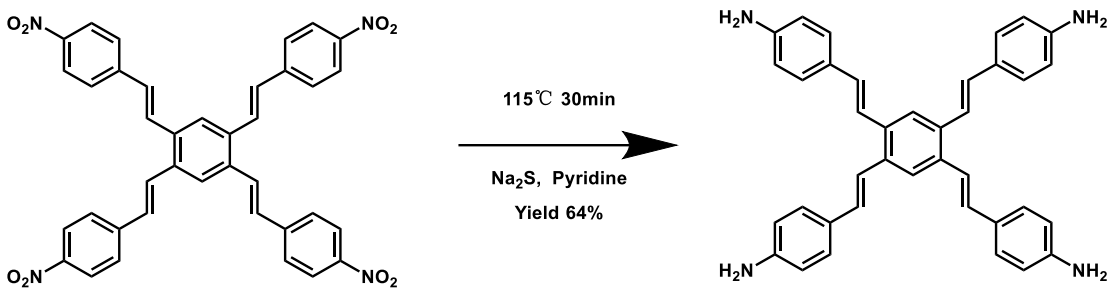

Figure S10. Synthetic routes of 1,2,4,5-tetrakis(p-aminostyryl)benzene.

In a nitrogen-flushed two-neck round-bottom flask equipped with a condenser and magnetic stir bar were combined 1,2,4,5-tetrakis(nitrophenylvinyl)benzene and pyridine. The mixture was heated to 130 °C (gentle reflux) and stirred for 10 min. Separately, a 1.5 M aqueous Na_2S solution was prepared by dissolving $Na_2S{\cdot}9H_2O$ (1.946 g, 0.00810 mol) in deionized water (5.4 mL). With the reaction mixture under nitrogen and stirring at 130 °C, the freshly prepared Na_2S solution was added slowly over ~5 min. The reaction was maintained at temperature for 30 min after the addition was complete. The mixture was quenched by carefully pouring in water (50 mL). After quench, the vessel was cooled in an ice–water bath to promote aggregation of the precipitated product. The solid was collected by filtration, washed successively with water (3 × 60 mL), methanol (3 × 30 mL), and dichloromethane (3 × 30 mL), and then lyophilized (freeze-dried) for 24 h to afford the product as an orange powder (0.233 g, 64% yield; based on starting 1,2,4,5-tetrakis(nitrophenylvinyl)benzene).^{1}H NMR (400 MHz, $(CD_3)_2SO$, ppm): δ = 7.78 (s, 2H), 7.26 (d, 4H), 7.06 (d, 4H), 7.37 (d, 8H), 6.59 (d, 8H) ,5.32 (s, 8H). ^{13}C NMR (101 MHz, DMSO-d6): δ (ppm) 149.17, 134.75, 131.17, 128.39, 125.80, 122.79, 120.56, 114.38.

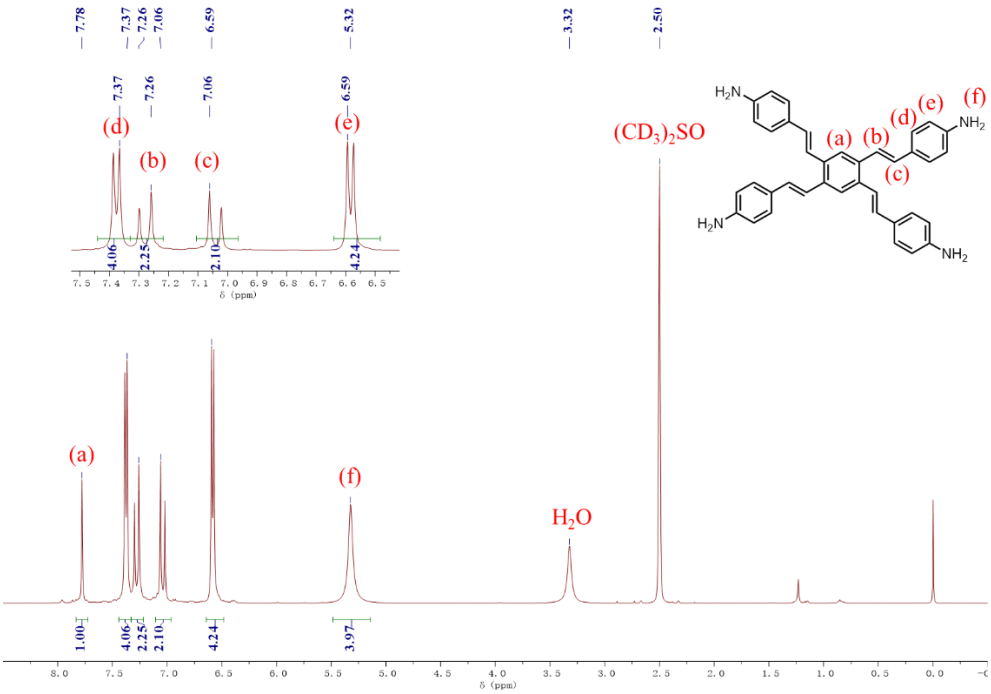

Figure S11. ^{1}H-NMR spectrum of 1,2,4,5-tetrakis(p-aminostyryl)benzene.

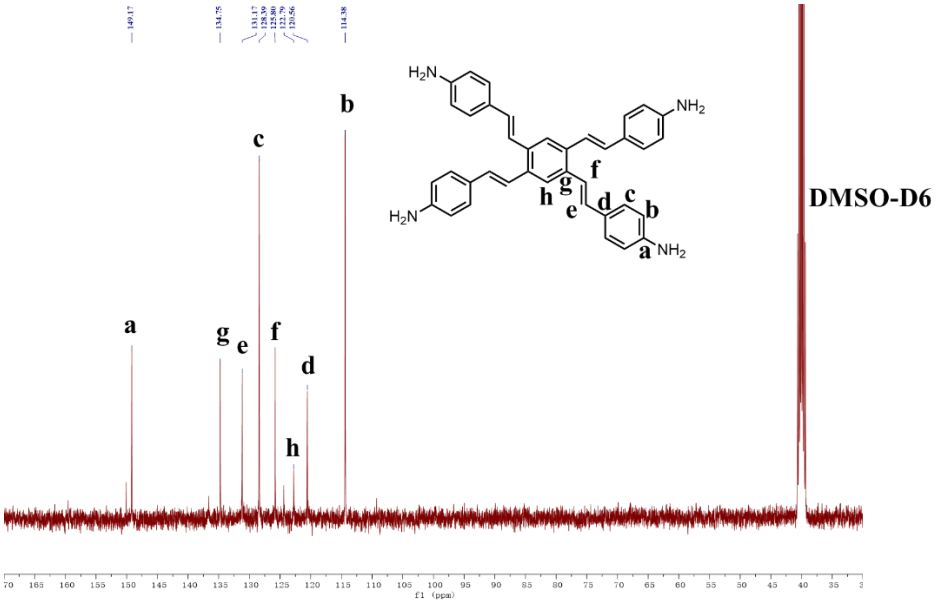

Figure S12. ^{13}C-NMR spectrum of 1,2,4,5-tetrakis(p-aminostyryl)benzene.

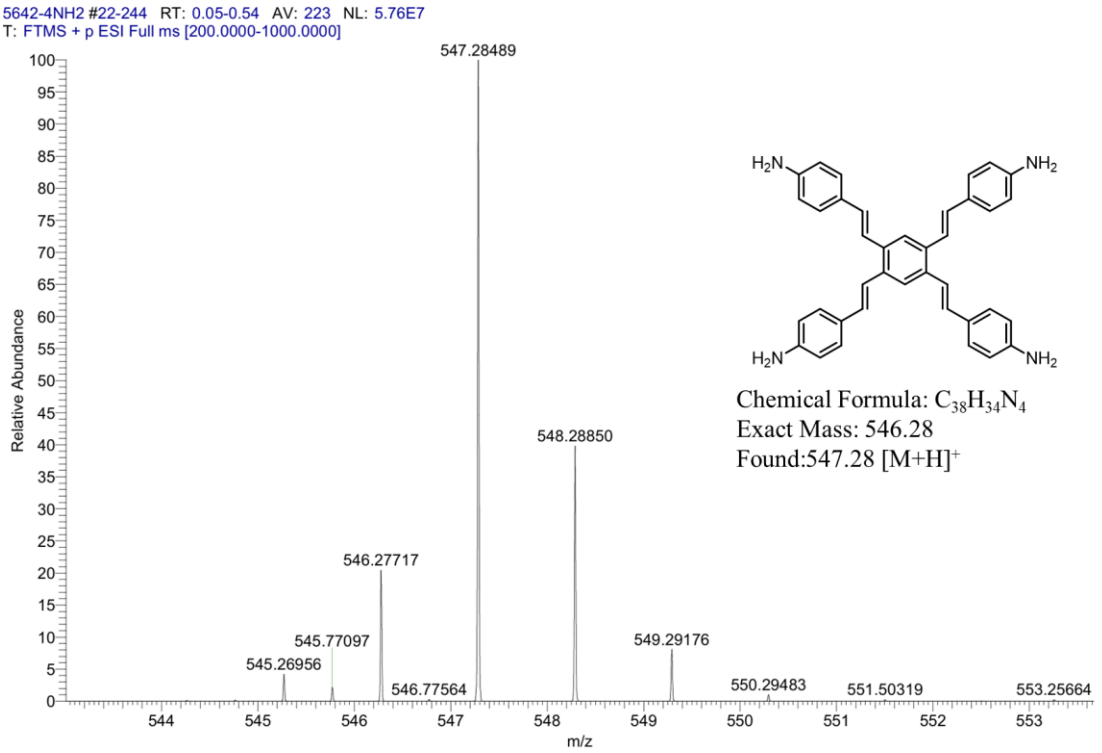

Figure S13. ESI mass spectrum of 1,2,4,5-tetrakis(p-aminostyryl)benzene.

Table S1.Elemental analysis data of monomers.

Name		N(%)	C(%)	H(%)	Formula
4A-NH_2	Found	9.89	81.12	6.26	$C_{38}H_{34}N_4 \cdot 0.88H_2O$
	Anal. Calcd .	9.96	81.13	6.41	
4A-CHO	Found	0	80.16	5.04	$C_{42}H_{30}O_4 \cdot 1.67H_2O$
	Anal. Calcd .	0	80.23	5.34	
4A-NO_2	Found	8.00	67.38	3.92	$C_{38}H_{26}N_4O_8 \cdot 0.67H_2O$
	Anal. Calcd .	8.26	67.26	4.06	

(a)

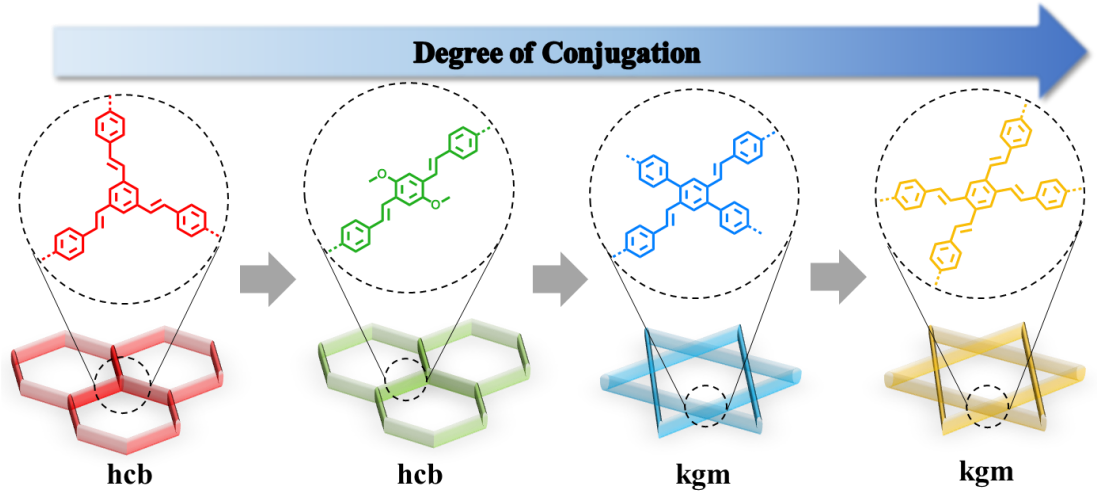

(b)

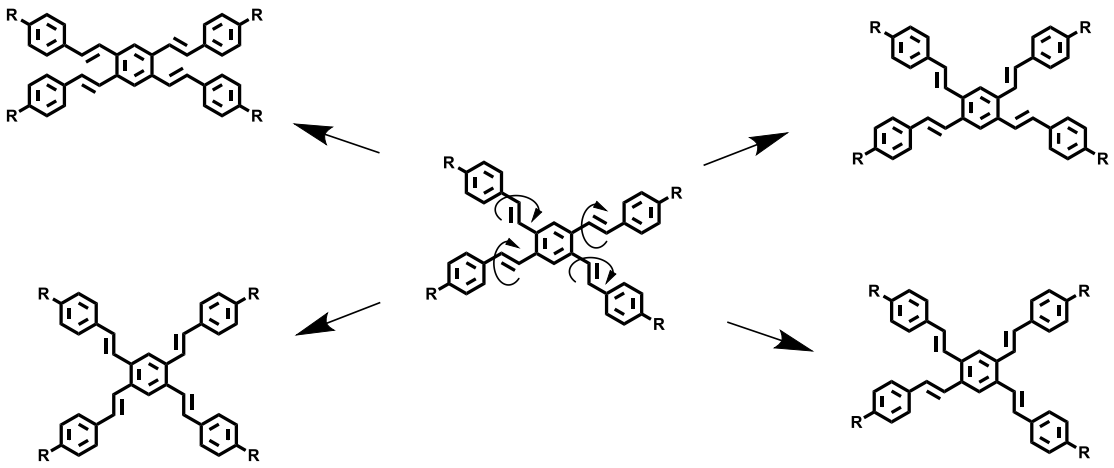

Figure S14. (a) Development of Oligo(Phenylenevinylene)-Based COFs.(b) Different conformations of tetra-armed oligo(phenylenevinylene) monomers.

Synthesis of COF-924-Sol

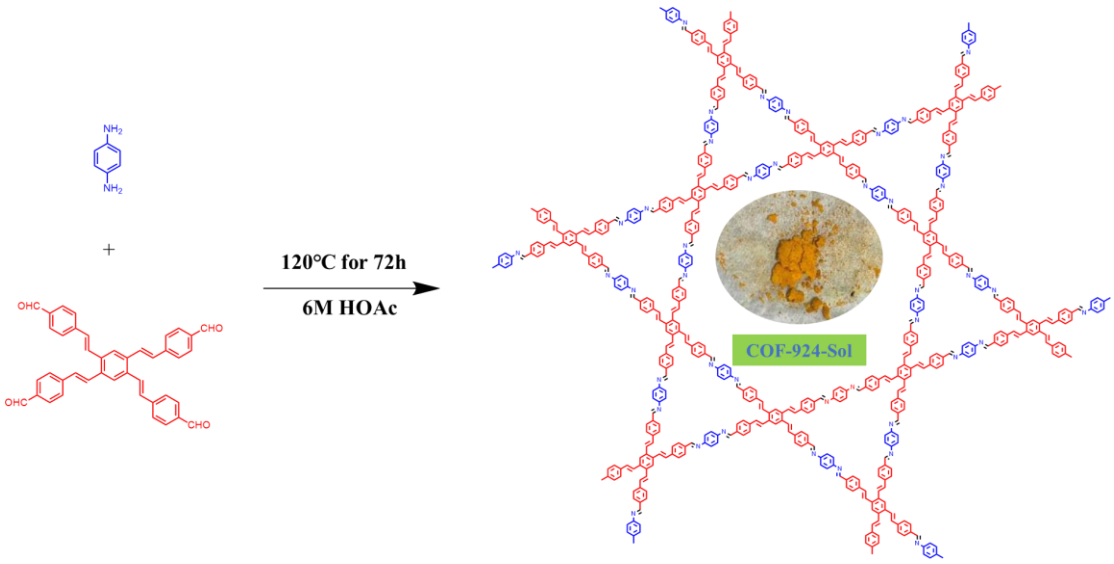

Figure S15. Synthetic routes of COF-924-Sol.

1,2,4,5-Tetrakis(p-formylstyryl)benzene solid(29.9 mg, 0.05 mmol) and p-phenylenediamine (10.8 mg, 0.1mmol) were added into a glass tube, then the mixture was dissolved in reaction solution (mesitylene/dioxane, v/v = 0.75 mL/0.25 mL, 0.5 mL /0.5 mL, 0.25 mL /0.75 mL, o-dichlorobenzene/n-butanol, v/v = 0.75 mL/0.25 mL, 0.5 mL /0.5 mL, 0.25 mL /0.75 mL), which were used to explore the best synthesis condition. the mixture was added 0.1 mL (6 M) HOAc aqueous solution. Then the tube was flash frozen in a liquid nitrogen bath and flame sealed degassed through three freeze-pump-thaw cycles and sealed under vacuum. Upon warming to room temperature, the ampoule was placed in an oven at 120 ºC and left undisturbed for 3 days. The resulting precipitate was filtered, exhaustively washed by methanol. The resulting solid was dried, and then subjected to Soxhlet extractions with THF and acetone for 1 day, respectively, to remove the trapped guest molecules. The solid was

washed by methanol for 12 h and then dried by supercritical CO_2. The powder was collected and dried under vacuum condition at 120 °C for 12 h to yield COF-924-Sol as a orange powder (14.3 mg, yield 48% in condition with Mes/Dio= 1:3).

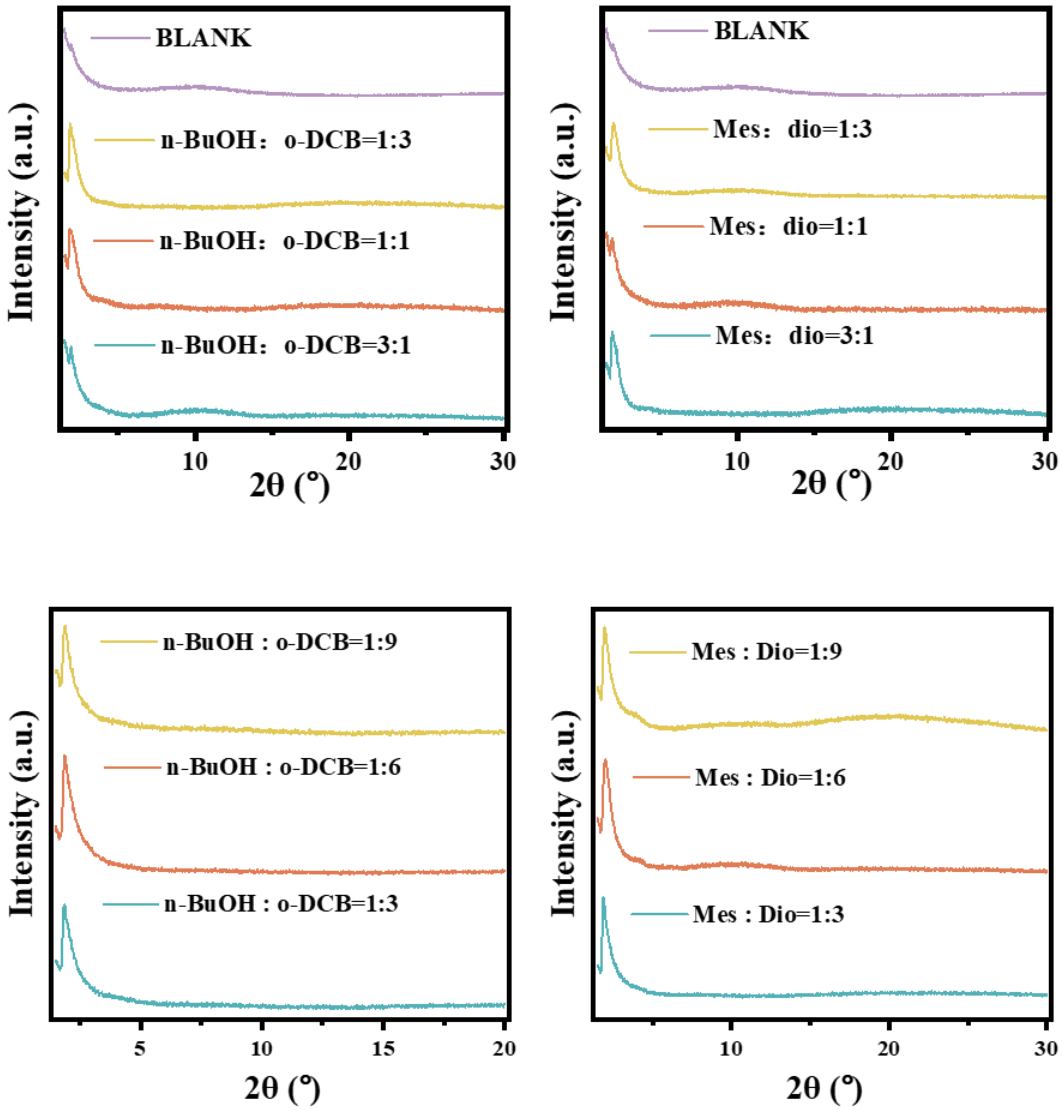

Figure S16. PXRD of COF-924-Sol synthesized in different reaction solution.

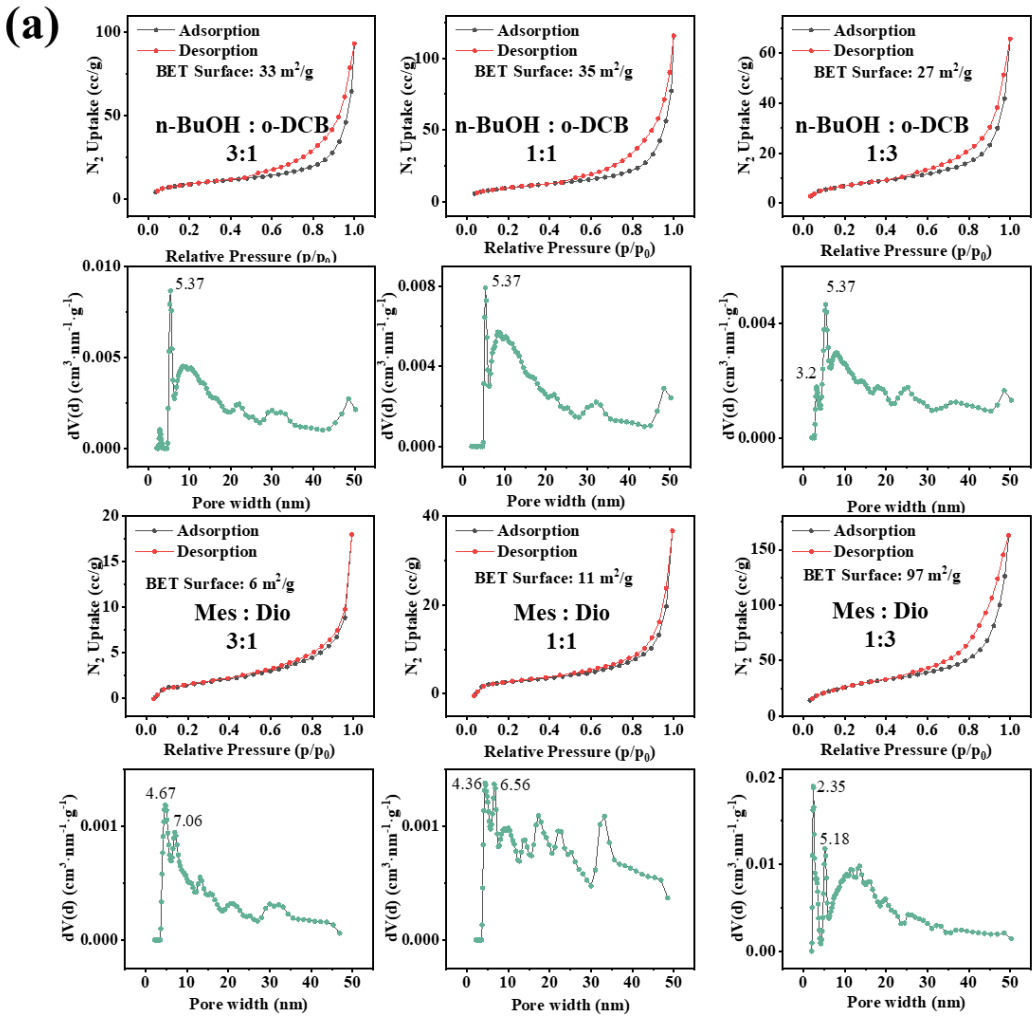

Figure S17. (a) N_2 adsorption-desorption isotherms of COF-924-Sol synthesized in different reaction solution.

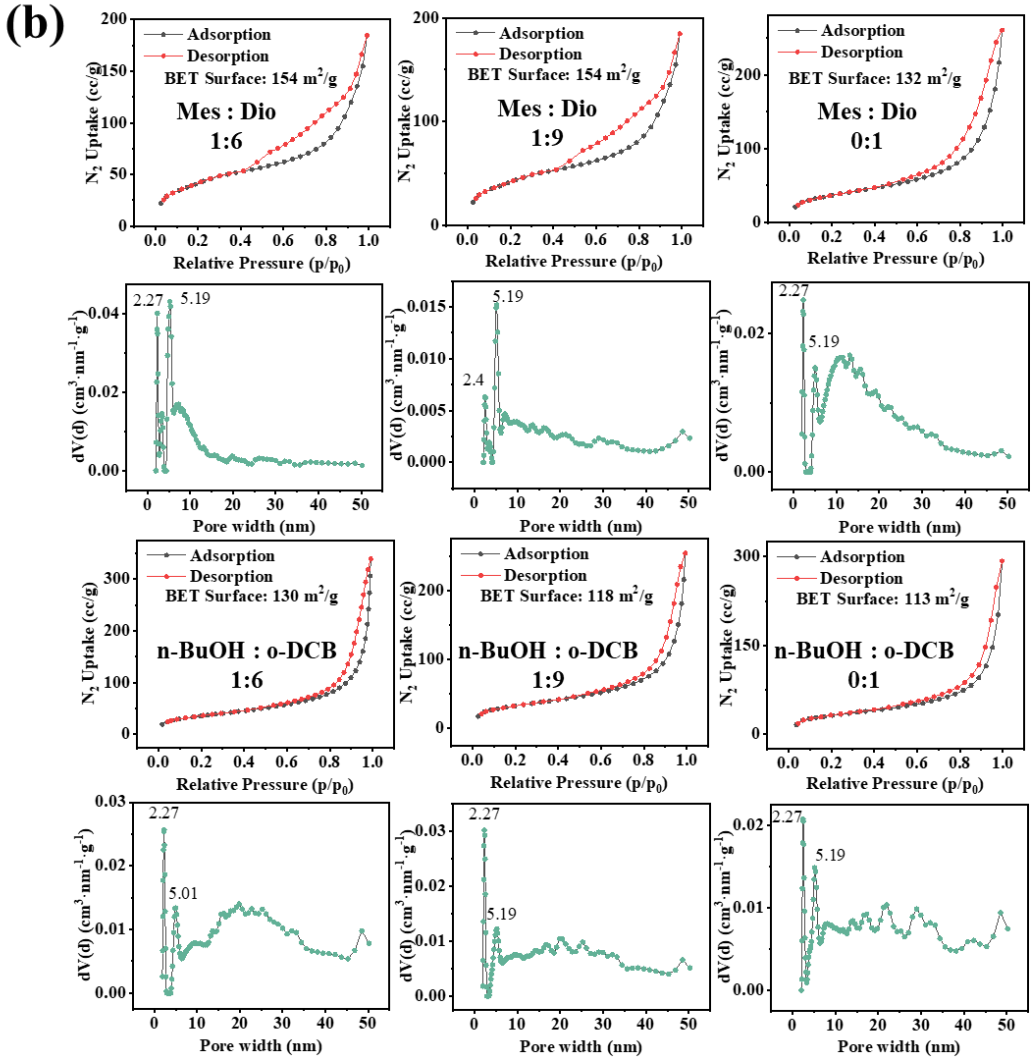

Figure S18. (b) N_2 adsorption-desorption isotherms of COF-924-Sol synthesized in different reaction solution.

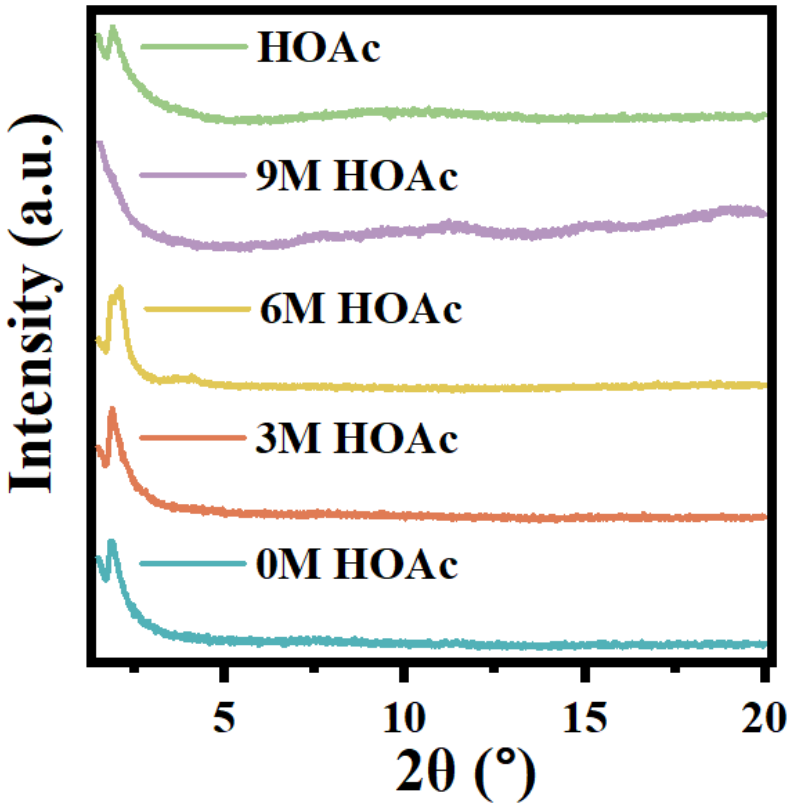

Figure S19. PXRD of COF-924-Sol synthesized in different acid concentration.

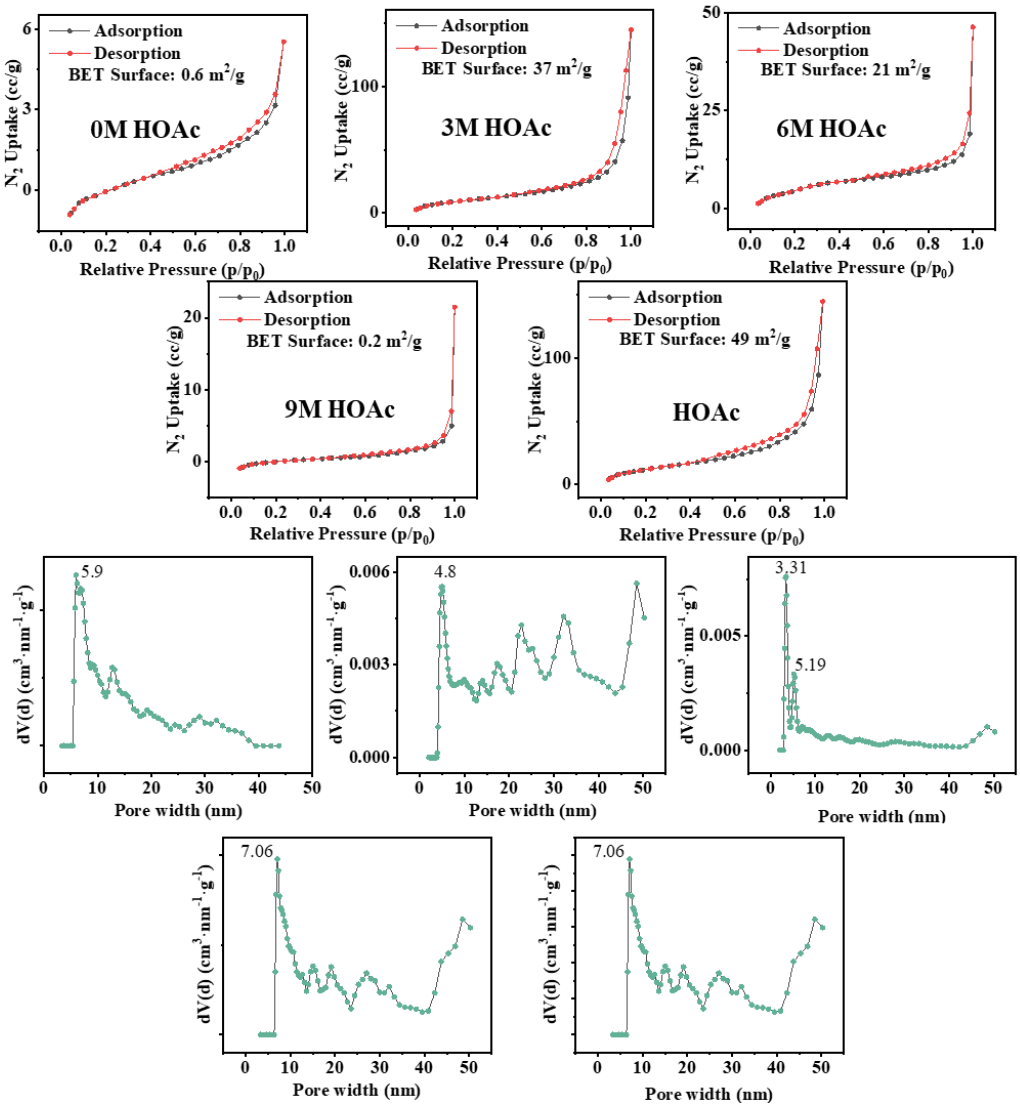

Figure S20. N_2 adsorption-desorption isotherms of COF-924-Sol synthesized in different acid concentration.

Synthesis of COF-942-Sol

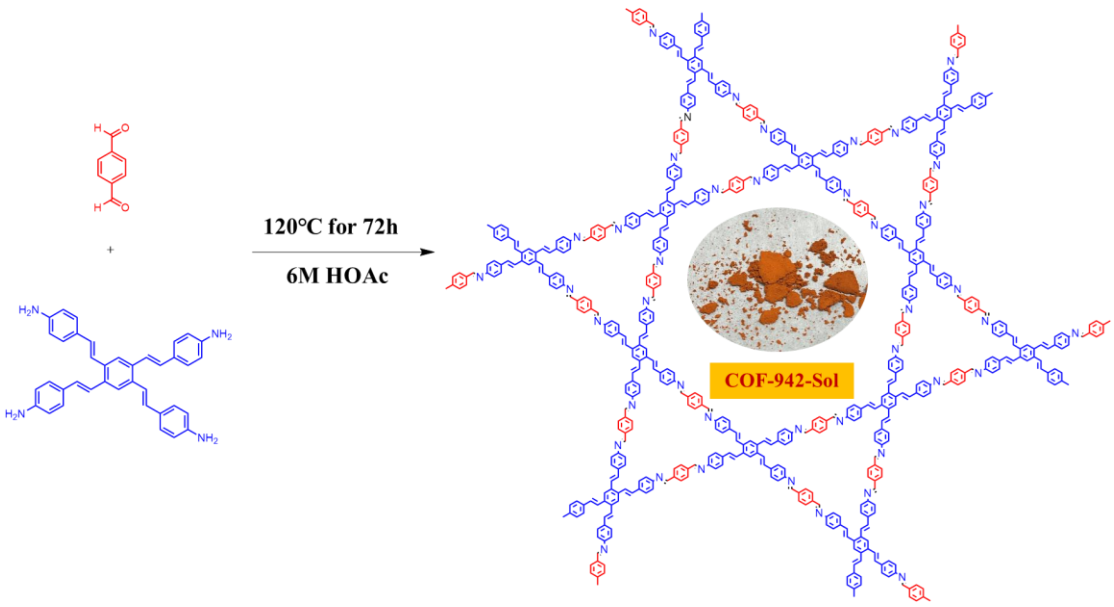

Figure S21. Synthetic routes of COF-942-Sol.

1,2,4,5-Tetrakis(p-aminostyryl)benzene solid (27.4 mg, 0.05 mmol) and terephthalaldehyde (13.4 mg, 0.1mmol) were added into a glass tube, then the mixture was dissolved in reaction solution (mesitylene/dioxane, v/v = 0.75 mL/0.25 mL, 0.5 mL /0.5 mL, 0.25 mL /0.75 mL, o-dichlorobenzene/n-butanol, v/v = 0.75 mL/0.25 mL, 0.5 mL /0.5 mL, 0.25 mL /0.75 mL), which were used to explore the best synthesis condition. the mixture was added 0.1 mL (6 M) HOAc aqueous solution. Then the tube was flash frozen in a liquid nitrogen bath and flame sealed degassed through three freeze-pump-thaw cycles and sealed under vacuum. Upon warming to room temperature, the ampoule was placed in an oven at 120 ºC and left undisturbed for 3 days. The resulting precipitate was filtered, exhaustively washed by methanol. The resulting solid was dried, and then subjected to Soxhlet extractions with THF and acetone for 1 day, respectively, to remove the trapped guest molecules. The solid was

washed by methanol for 12 h and then dried by supercritical CO_2. The powder was collected and dried under vacuum condition at 120 °C for 12 h to yield COF-942-Sol as a scarlet powder (24.8mg, yield 67% in condition with o-dichlorobenzene/n-butanol = 1:3).

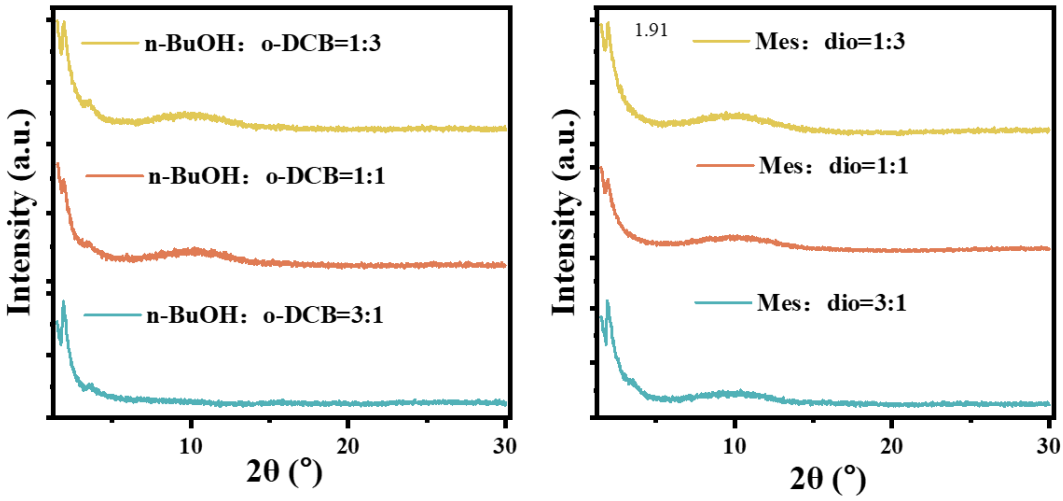

Figure S22. PXRD of COF-942-Sol synthesized in different reaction solution.

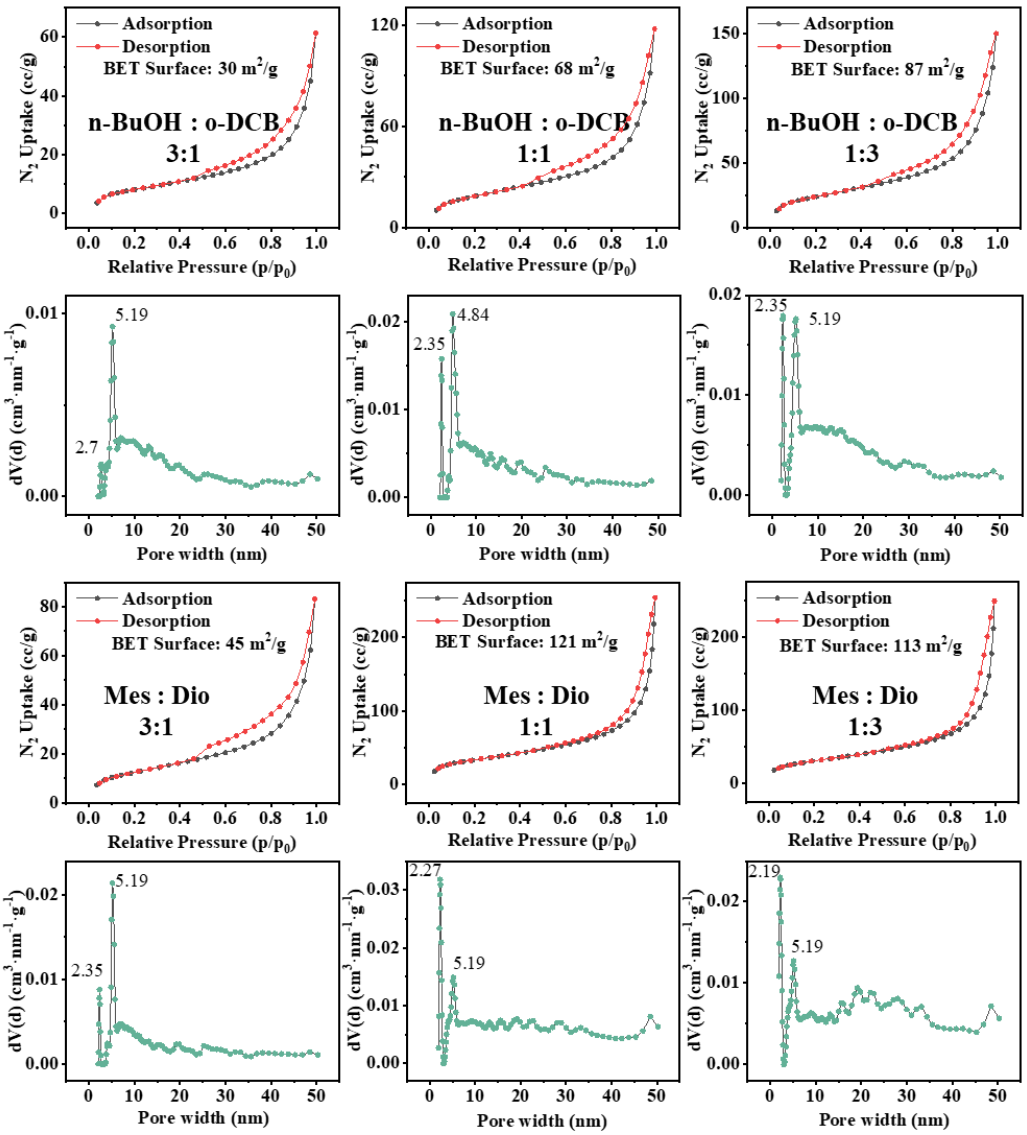

Figure S23. N_2 adsorption-desorption isotherms of COF-942-Sol synthesized in different reaction solution.

Synthesis of COF-924

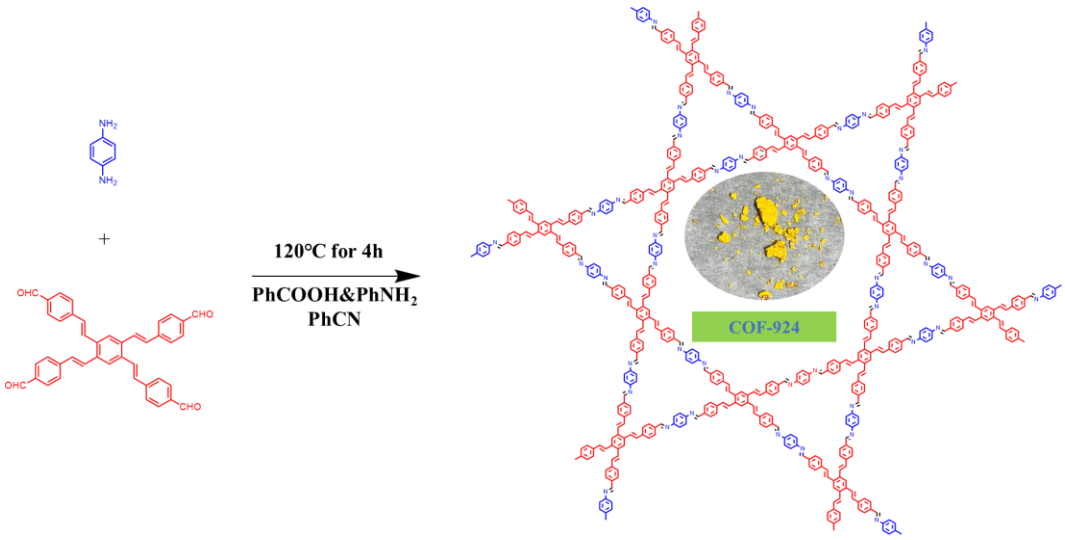

Figure S24. Synthetic routes of COF-924.

In a 20 mL screw-cap reaction vial, benzoic acid (1.000 g, 8.20 mmol) was dissolved in benzonitrile (3.214 mL) by heating on a 120 °C aluminum block; to the hot solution were added 1,2,4,5-tetrakis(p-formylstyryl)benzene (29.9 mg, 0.050 mmol) and an aniline solution (0.7 M in benzonitrile, 1.786 mL, 1.25 mmol), and the mixture was heated at 120 °C until homogeneous, after which a p-phenylenediamine solution (0.1 M in benzonitrile, 1.00 mL, 0.100 mmol) was introduced; the vial was sealed, left undisturbed (no stirring) at 120 °C for 4 h to allow COF formation, then cooled to room temperature and treated with methanol to induce precipitation; the suspension was centrifuged, the supernatant decanted, and the solid washed with methanol, transferred to teabags, Soxhlet-extracted sequentially with THF (24 h) and acetone (24 h), washed with methanol (12 h), dried by supercritical CO2, and finally dried under vacuum at 120 °C for 12 h to afford COF-924 as a powder (12.0 mg, 32% yield based on 1,2,4,5-tetrakis(p-formylstyryl)benzene).

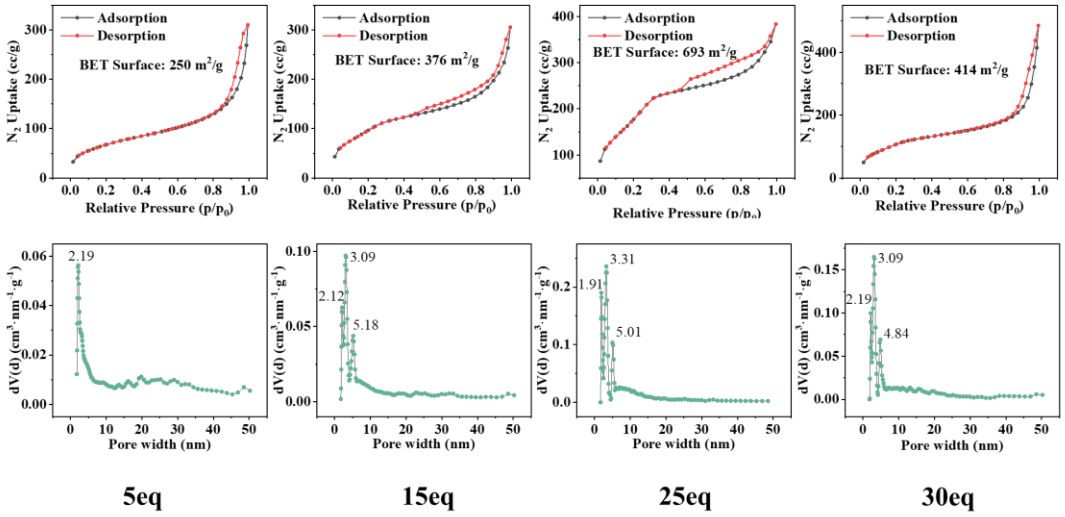

Figure S25. (a) N_2 adsorption-desorption isotherms of COF-924 synthesized in different equivalents of aniline.

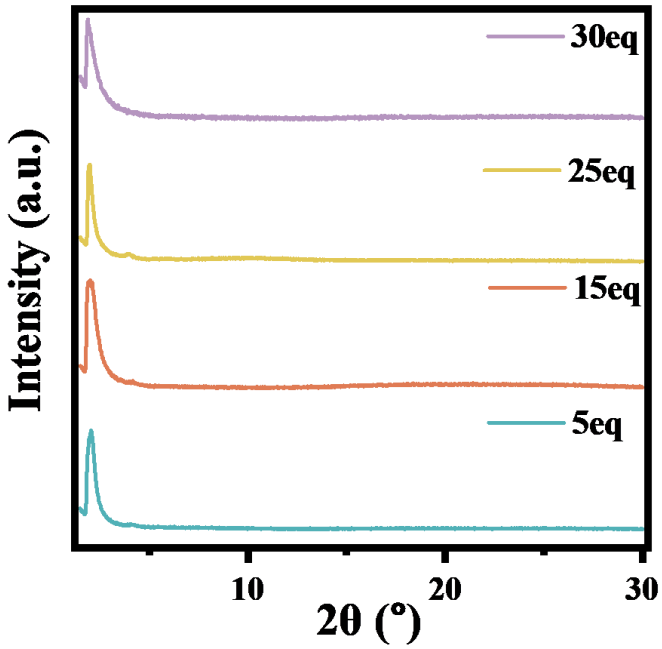

Figure S26. (b)PXRD of COF-924 synthesized in different equivalents of aniline.

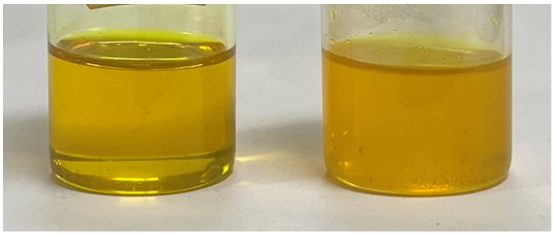

Figure S27. The tetra-armed monomer was dissolved in benzonitrile, with and without aniline.

Synthesis of COF-942

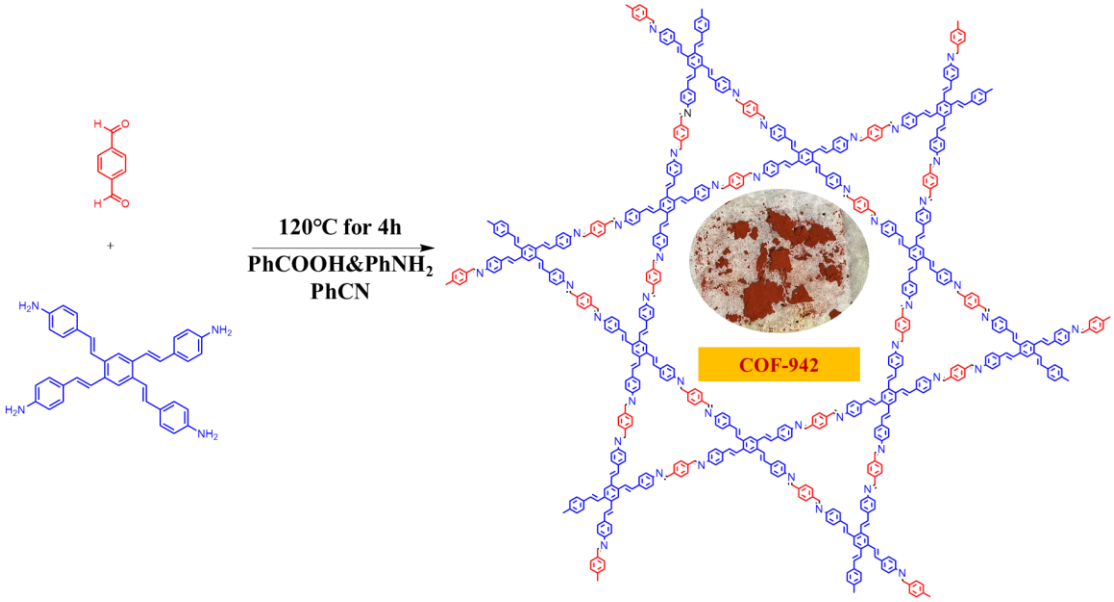

Figure S28. Synthetic routes of COF-942.

In a 20 mL screw-cap reaction vial, benzoic acid (1.000 g, 8.20 mmol) was dissolved in benzonitrile (4.286 mL) by heating on a 120 °C aluminum block; to the hot solution were added terephthalaldehyde (13.4 mg, 0.10 mmol) and an aniline solution (0.7 M in benzonitrile, 0.714 mL, 0.50 mmol), and the mixture was heated at 120 °C until

homogeneous, after which a benzonitrile solution (1.00 mL) of 1,2,4,5-tetrakis(p-aminostyryl)benzene (27.4 mg, 0.050 mmol) was introduced; the vial was sealed and left undisturbed (no stirring) at 120 °C for 4 h, then cooled to room temperature and treated with methanol to induce precipitation; the suspension was centrifuged, the supernatant decanted, and the solid washed with methanol, transferred to teabags, Soxhlet-extracted sequentially with THF (24 h) and acetone (24 h), washed with methanol (12 h), dried by supercritical CO_2, and finally dried under vacuum at 120 °C for 12 h to afford COF-942 as a powder (31.1 mg, 84% yield based on 1,2,4,5-tetrakis(p-aminostyryl)benzene).

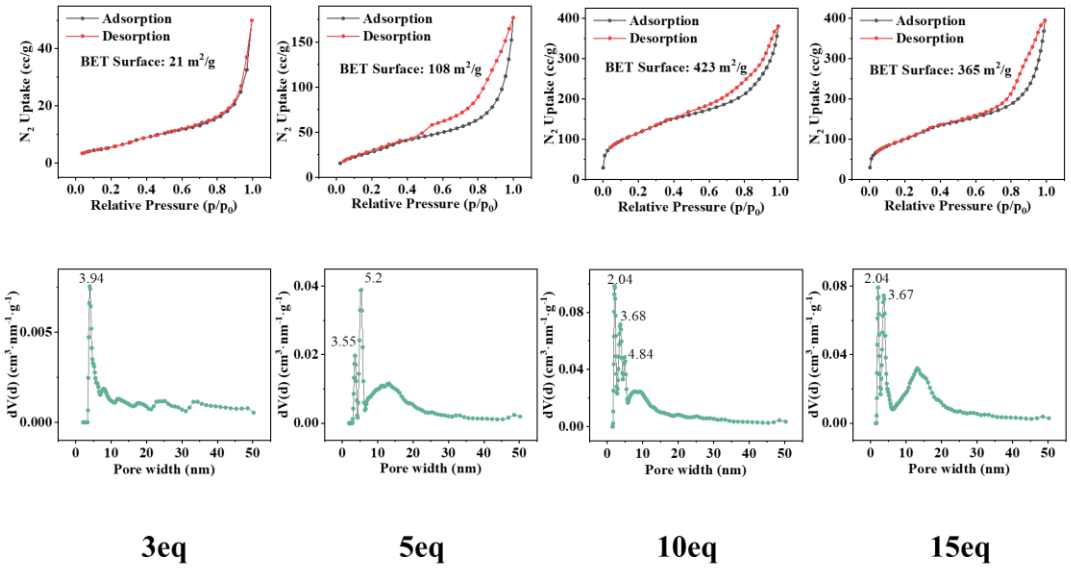

Figure S29. (a) N_2 adsorption-desorption isotherms of COF-942 synthesized in different equivalents of aniline.

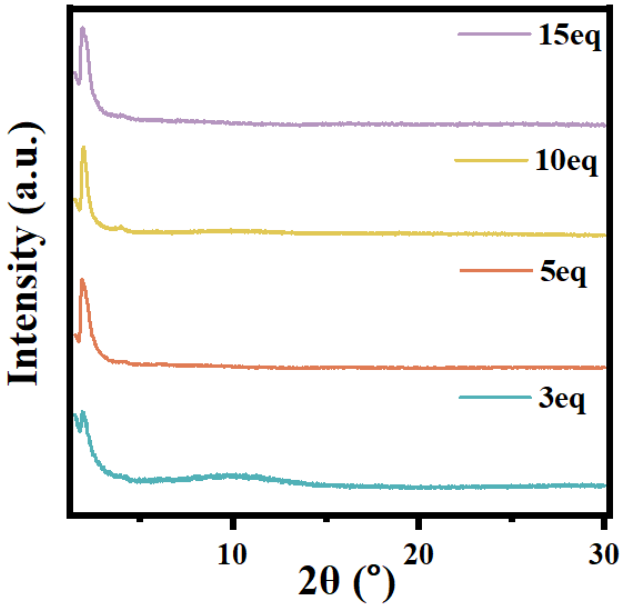

Figure S30. PXRD of COF-942 synthesized in different equivalents of aniline.

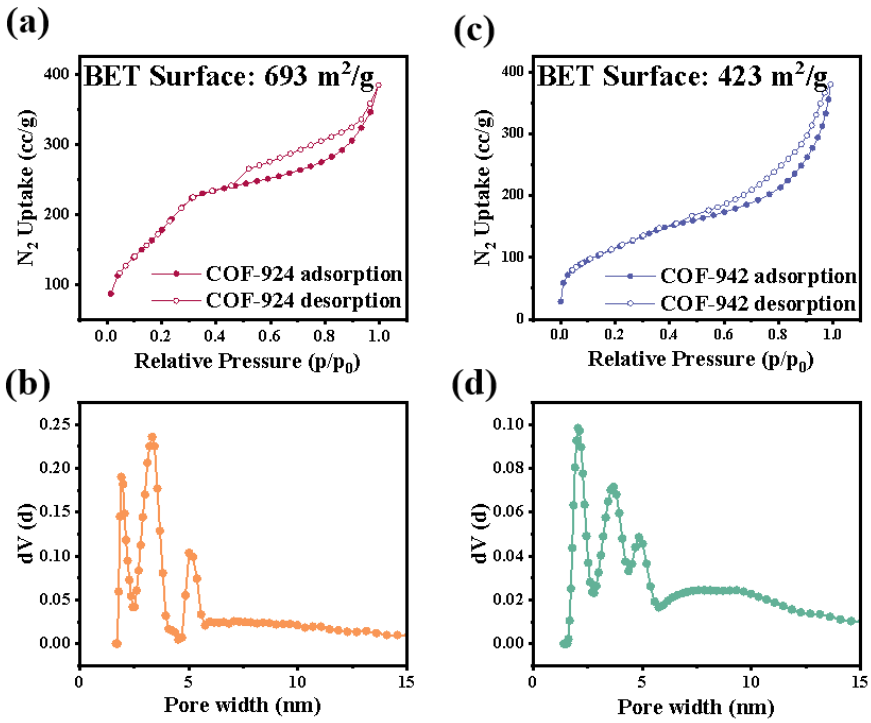

Figure S31. (a, c) Nitrogen adsorption-desorption isotherms of COF-924 and COF-942 at 77 K; (b, d) pore size distribution profiles (QSDFT) of COF-924 and COF-942.

Section S3. Characterization data

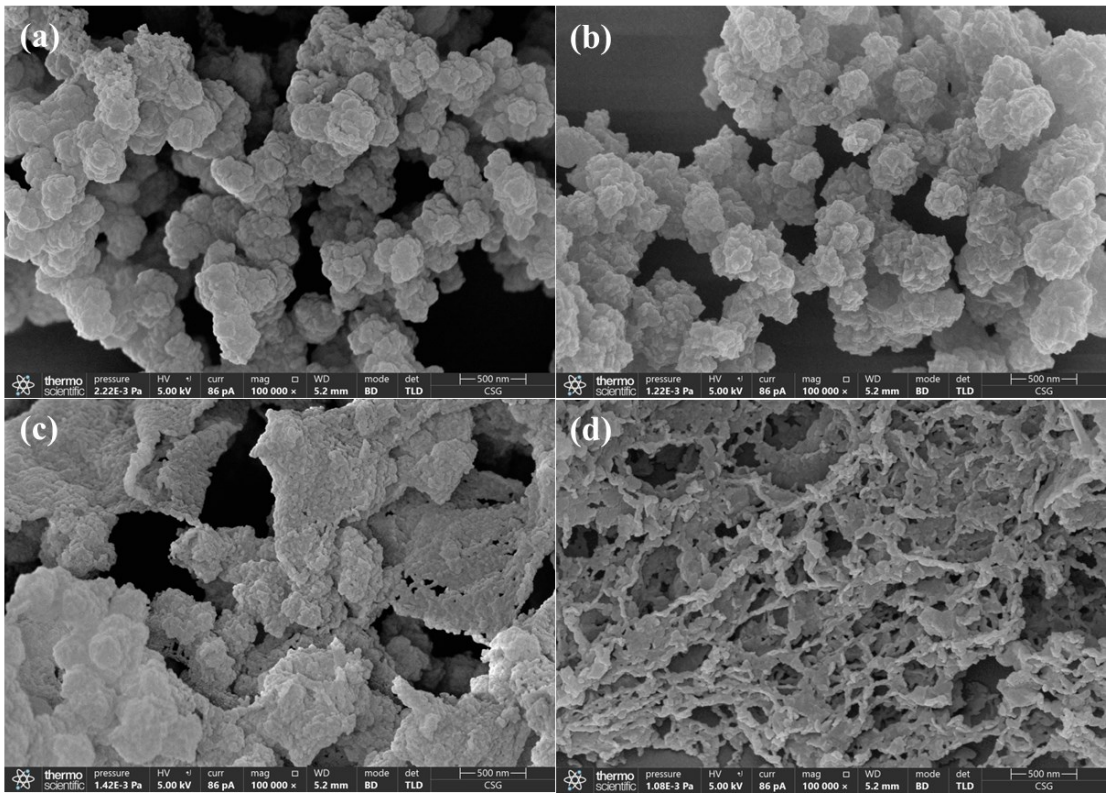

Figure S32. SEM images of all COFs: (a) COF-924, (b) COF-942, (c) COF-924-Sol, (d) COF-942-Sol.

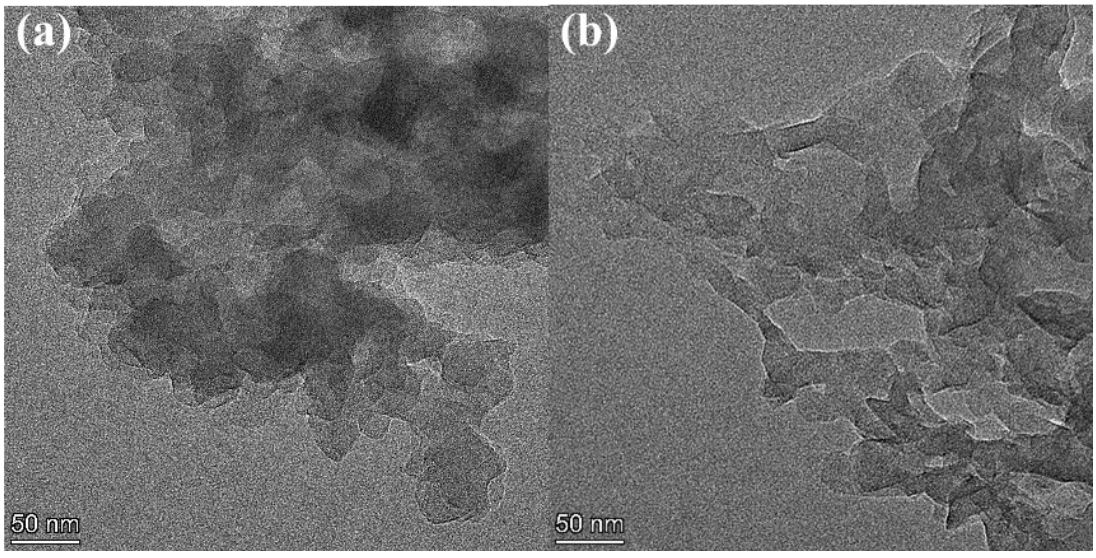

Figure S33. TEM images of COFs: (a) COF-924-Sol, (b) COF-942-Sol.

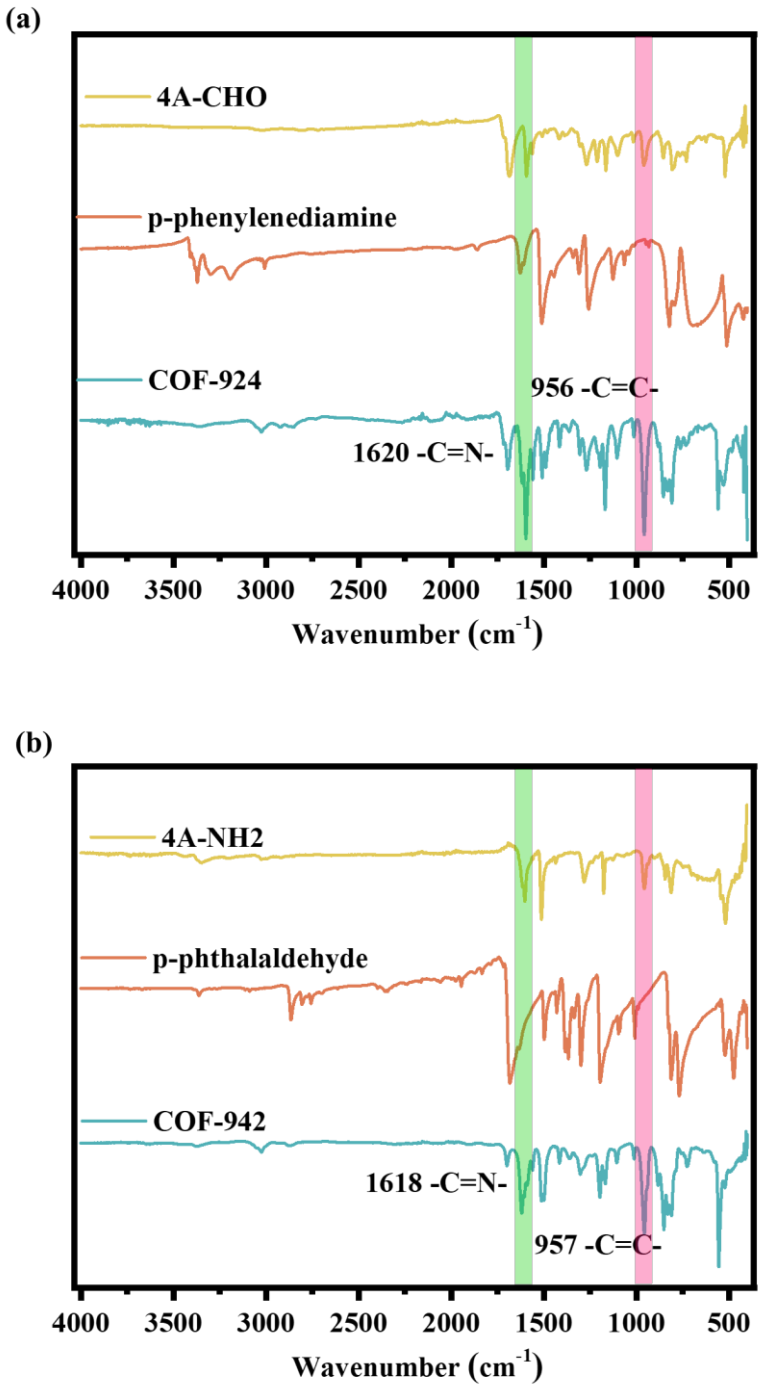

Figure S34. (a) Fourier transform infrared spectroscopy (FT-IR) of COF-924 and (b)Fourier transform infrared spectroscopy (FT-IR) of COF-942.

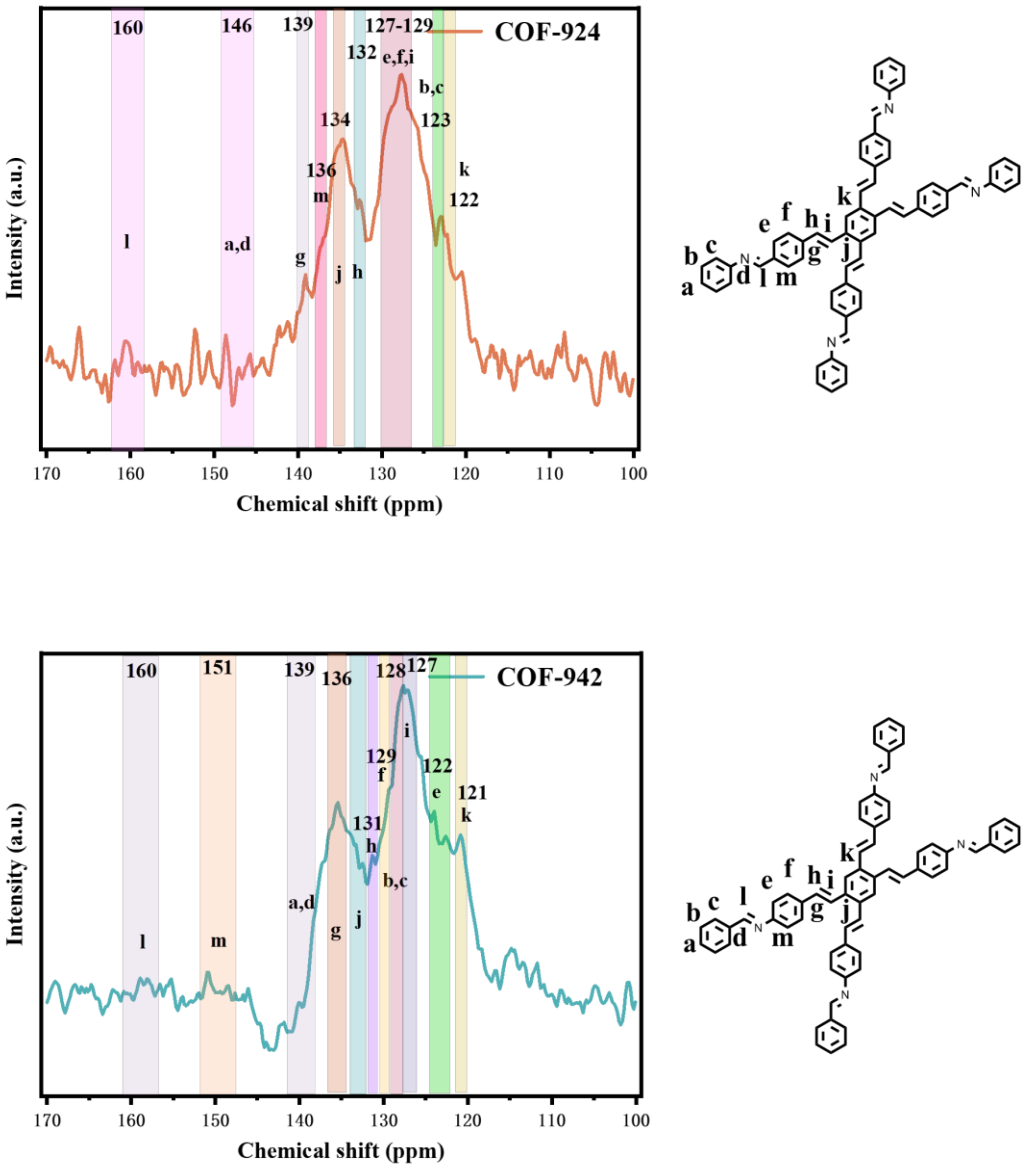

Figure S35. Solid state ^{13}C CP/MAS NMR spectrum of COF-924 and COF-942 powder.

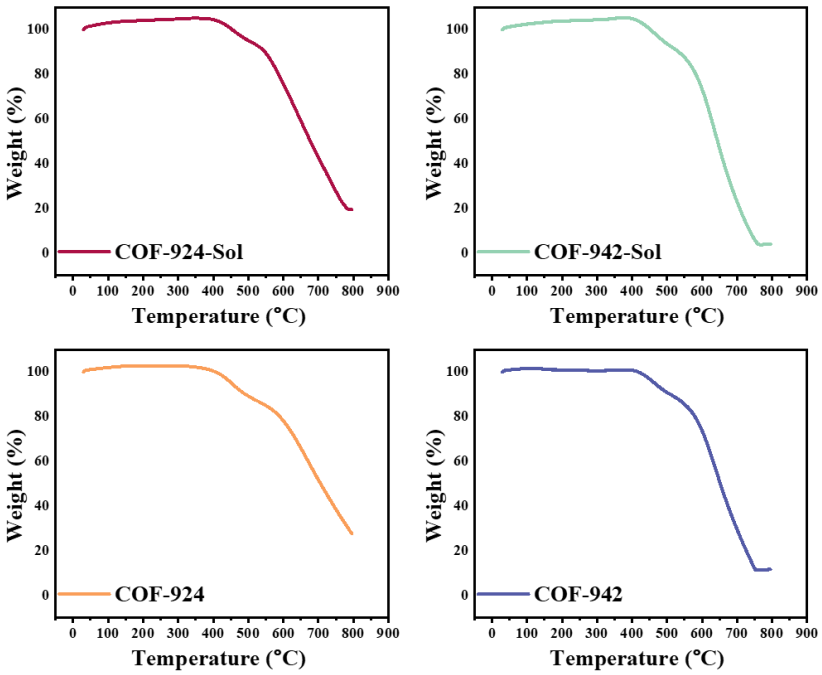

Figure S36. Thermogravimetric analysis curve for COF-924 and COF-942 powder. All of them are stable up to 400 °C.

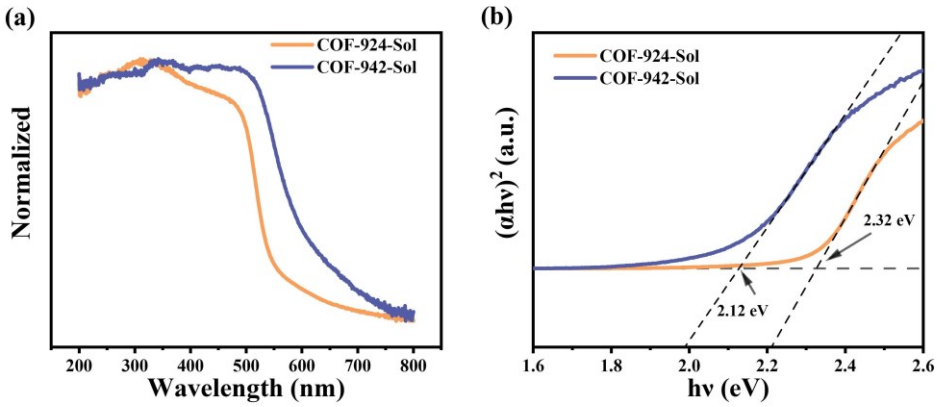

Figure S37. (a) UV–vis absorption spectra and (b) Tauc plots for COF-924-Sol and COF-942-Sol.

For protonation by AC, the COF sample (5 mg) was homogenously suspended in 2 mL of 0.1 M AC under ambient conditions with magnetic stirring, after which phase segregation was achieved via centrifugation to isolate the solid-phase catalyst.

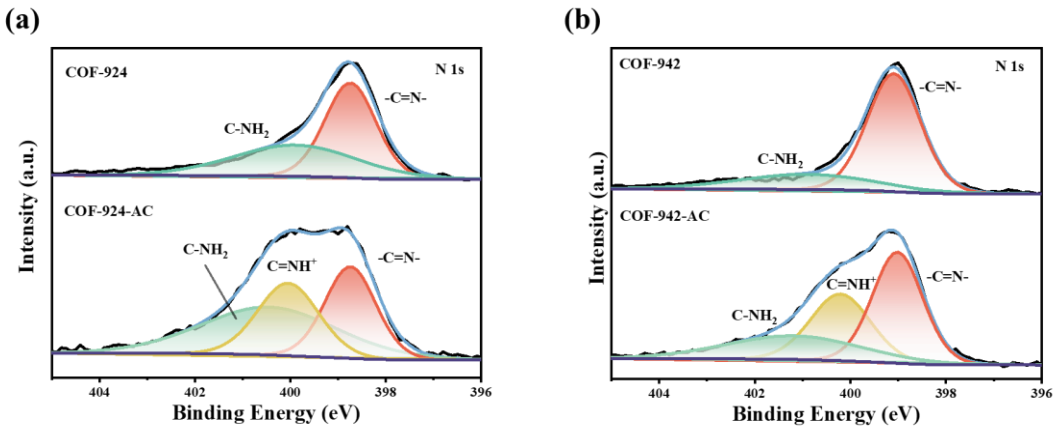

Figure S38. X-ray photoelectron spectroscopy of protonated COFs: (a) COF-924, COF-924-AC, (b) COF-942, COF-942-AC.

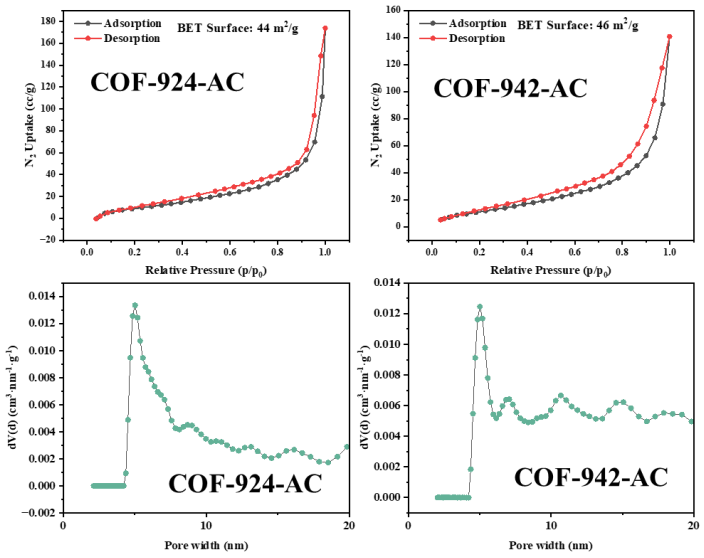

Figure S39. N_2 adsorption-desorption isotherms and pore distributions of protonated COFs.

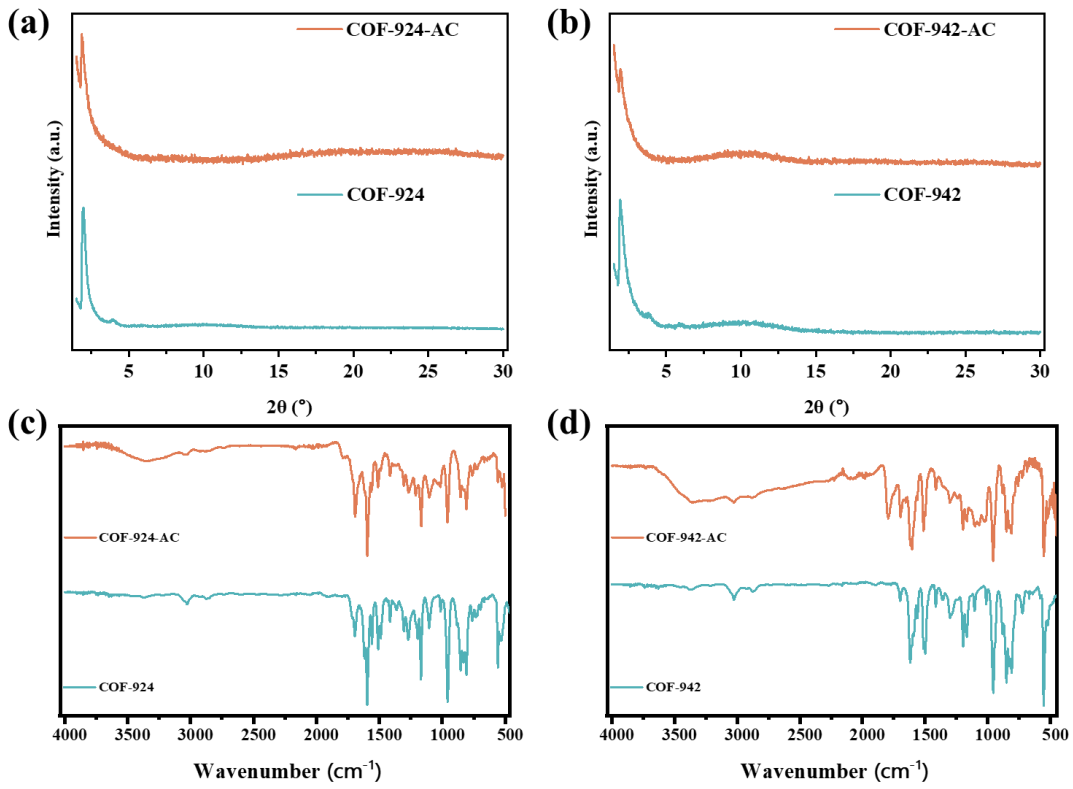

Figure S40. (a) and (b) PXRD patterns of initial COF-924, COF-942, and protonated COF-924-AC and COF-942-AC. (c) and (d) FT-IR spectra of initial COF-924, COF-942, and protonated COF-924-AC and COF-942-AC.

Section S4. Photocatalytic measurements

Photocatalytic hydrogen evolution reaction measurements

5 mg photocatalyst was dispersed into 50 mL 0.1 M ascorbic acid solution and then added into the photoreactor. Then the resulting suspension was ultrasonicated for 30 min to obtain a well dispersed suspension. Pt was loaded on the surface of the photocatalyst by using H_2PtCl_6 in the in situ photodeposition approach. We evacuated the mixture several times to remove air completely before irradiation under a 300 W Xe-lamp and a water-cooling filter. The temperature of the reaction solution was kept

at room temperature by a flow of cooling water. The generated gases were analyzed by gas chromatography equipped with a thermal conductive detector (TCD) with argon as the carrier gas. The light resource was changed by using different cut-off filters. A 420 nm cut-off filter was used to obtain visible light.

AQY measurements

Apparent quantum efficiency (AQY) measurements were performed under monochromatic irradiation, generated from a 300 W Xe lamp equipped with bandpass filters (central wavelength: 420, 450, 520, 550, 600, 700 nm; full width at half maximum: 10 nm). Monochromatic photon fluxes at each wavelength were measured using an optical photodiode power meter (CEL-NP2000), the intensities were 75, 78, 73, 72, 81, 80 $W \cdot m^{-2}$, respectively. The AQY was calculated using the following equation:

$$AQY = \frac{N_e}{N_P} \times 100\% = \frac{10^9(v \times N_A \times n) \times (h \times c)}{P \times A \times \lambda} \times 100\%$$

Where, N_e is the amount of generated electron, N_p is the incident photons, v is the H_2 evolution rate ($mol \cdot s^{-1}$), N_A is Avogadro constant (6.022×10^{23} mol^{-1}), n is number of transferred electrons in hydrogen evolution reaction (2), h is the Planck constant (6.626×10^{-34} J·s), c is the speed of light (3×10^8 $m \cdot s^{-1}$), P is the intensity of irradiation light ($W \cdot m^{-2}$), A is the irradiation area (m^2), , t is the photoreaction time (s), λ is the wavelength of the monochromatic light (nm).

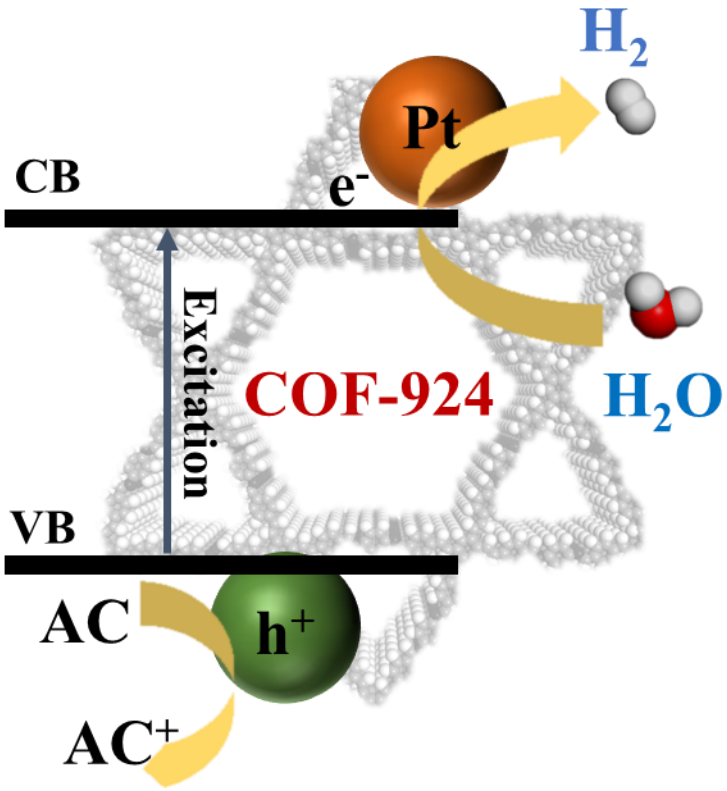

Scheme S1. Schematic illustration of the hydrogen evolution mechanism. Mechanistically, upon light absorption, the COF acts as the light-harvesting unit, generating excitons that can dissociate into electron–hole pairs. The photogenerated electrons are transferred from the COF conduction band to the Pt nanoparticles, where they reduce protons to produce H_2, while the holes remaining in the COF valence band are scavenged by the sacrificial electron donor (ascorbic acid in our work). The designed π-conjugated framework and imine linkage orientation in COF-924 facilitate efficient exciton dissociation and charge separation, whereas the porous structure promotes uniform dispersion of Pt, thereby increasing the number of accessible active sites and enhancing the overall hydrogen evolution rate. Details could also be found in the references, such as Adv. Mater. 2024, 2413118, and Nat. Rev. Mater. 2017, 2, 17050.

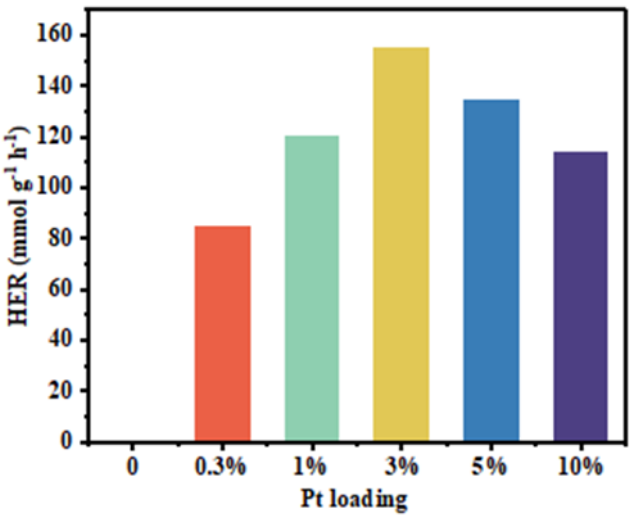

Figure S41. H_2 evolution of COF-924 under different contents of Pt loading within one hour.

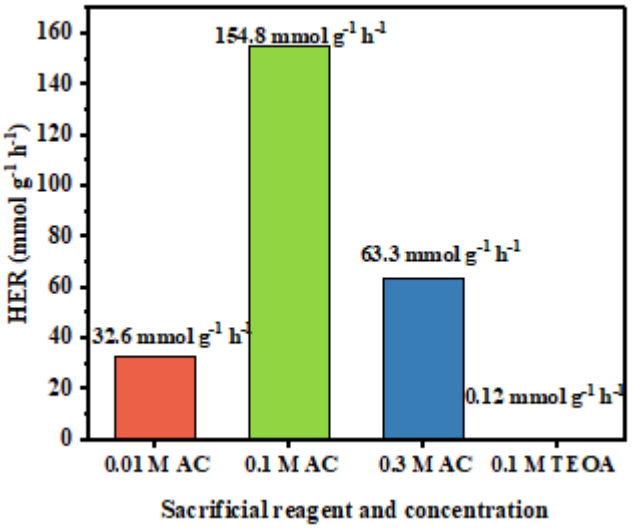

Figure S42. H_2 evolution of COF-924 in ascorbic acid (AC) and triethanolamine (TEOA).

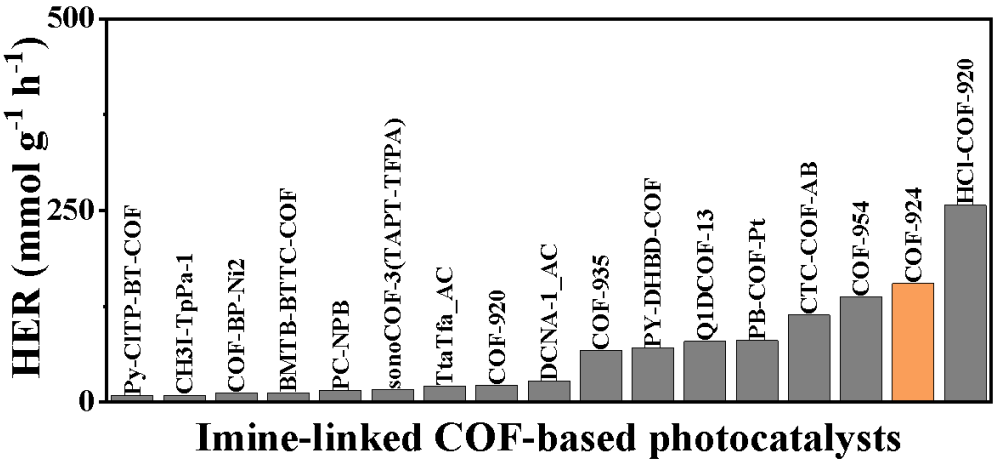

Figure S43. HER comparison of reported COFs.

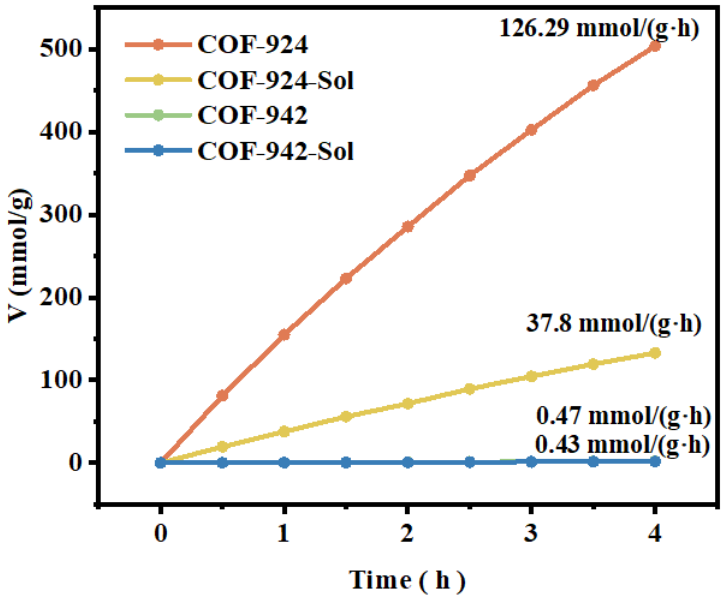

Figure S44. Photocatalytic hydrogen evolution performance of conventional solvothermal COF-924-Sol and COF-942-Sol, and controlled growth COF-924 and COF-942.

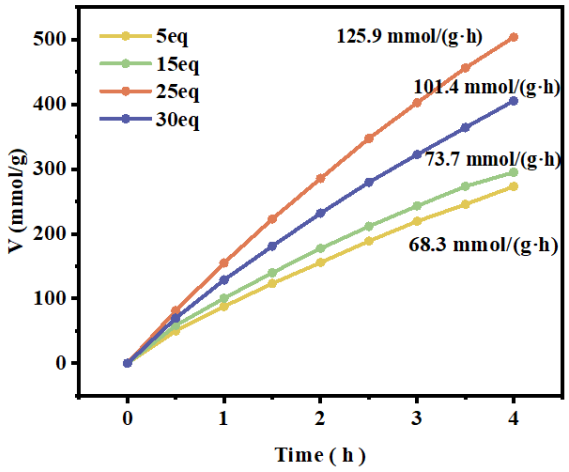

Figure S45. Photocatalytic hydrogen evolution performance of COF-924 prepared in different synthetic conditions.

Section S5. Characterization after photocatalysis

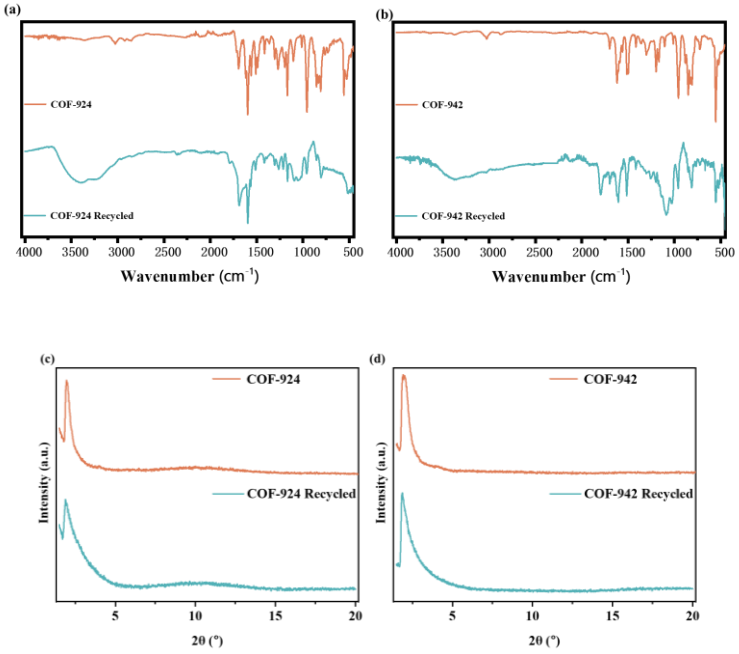

Figure S46. (a) and (b) FT-IR spectra of initial COF-924, COF-942, and recycled COF-924 and COF-942 after photocatalysis. (c) and (d) PXRD patterns of initial COF-924, COF-942, and recycled COF-924 and COF-942 after photocatalysis.

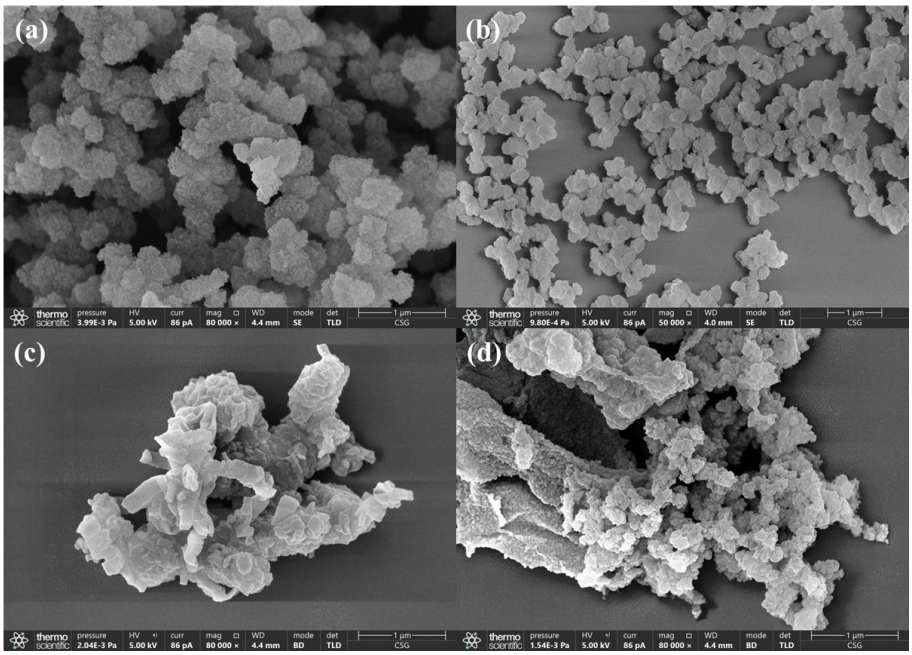

Figure S47. SEM images of recycled COF-942 (a), recycled COF-924 (b), recycled COF-942-Sol (c), and recycled COF-924- Sol (d).

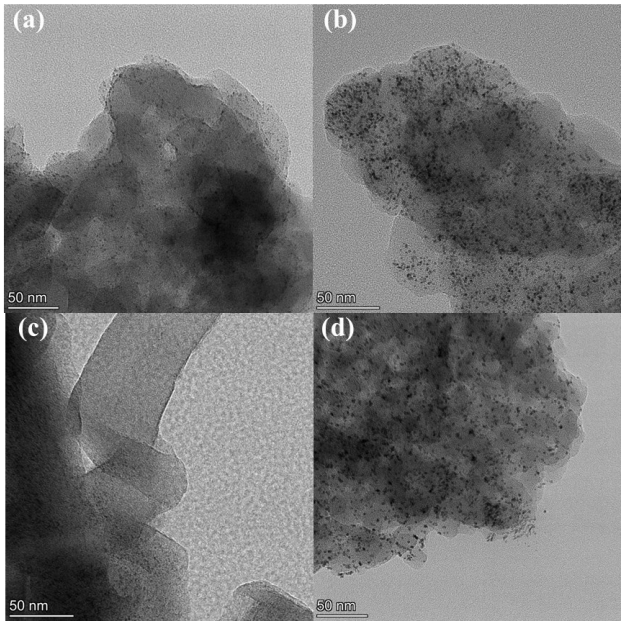

Figure S48. HRTEM images of recycled COF-942 (a), recycled COF-924 (b), recycled COF-942-Sol (c), and recycled COF-924-Sol (d).

Section S6. Electrochemical measurements

Indium-tin oxide (ITO) glasses were firstly cleaned by sonication in ethanol and acetone for 30 min and dried under nitrogen flow. 5 mg of COF powder was mixed with 1 mL ethanol and ultra-sonicated for 30 min to get a slurry. Then 50 μL 5% Nafion was added into the slurry for another 30 min ultra-sonication. The slurry was spreading onto ITO glass. After air drying, the boundary of the electrode was covered with an effective area of 1 cm^2. A conventional three electrodes cell was used with a platinum sheet (1 cm^{-2}) as the counter electrode and an Ag/AgCl electrode (saturated KCl) as reference electrode. The electrolyte was a 0.2 M Na_2SO_4 aqueous solution (pH 6.8). The working electrodes were immersed in the electrolyte for 60 s before any measurements were taken. The photocurrent measurements were conducted with a CHI760e workstation, with the working electrodes irradiated from the front side. The visible light was generated by a 300W xenon lamp (CEL-HXF300, Beijing China Education Au-light Co., Ltd) with a 420 nm cut-off filter, and was chopped manually. For Mott-Schottky experiments, the perturbation signal was 5 mV with the frequency from 1000-5000 Hz. The electrochemical impedance spectra (EIS) were performed in dark at open-circuit voltage with AC amplitude of 5 mV in the frequencies range of 0.1 Hz to 10^5 Hz.

The applied potential vs. Ag/AgCl is converted to RHE potentials using the following equation:

$$E_{RHE} = E_{\frac{Ag}{AgCl}} + 0.0591\ pH + E^{\theta}_{\frac{Ag}{AgCl}} \left(E^{\theta}_{\frac{Ag}{AgCl}} = 0.199\ V \right)$$

Tauc plot.

It is used to determine the optical bandgap of a semiconductor material. The plot is constructed by plotting the absorption coefficient (α) against the photon energy (hv). And it is a linear plot that can be extrapolated to the x-axis to determine the energy bandgap (Eg) of the material.

$$(ahv)^{\frac{1}{n}} = A(hv - E_g)$$

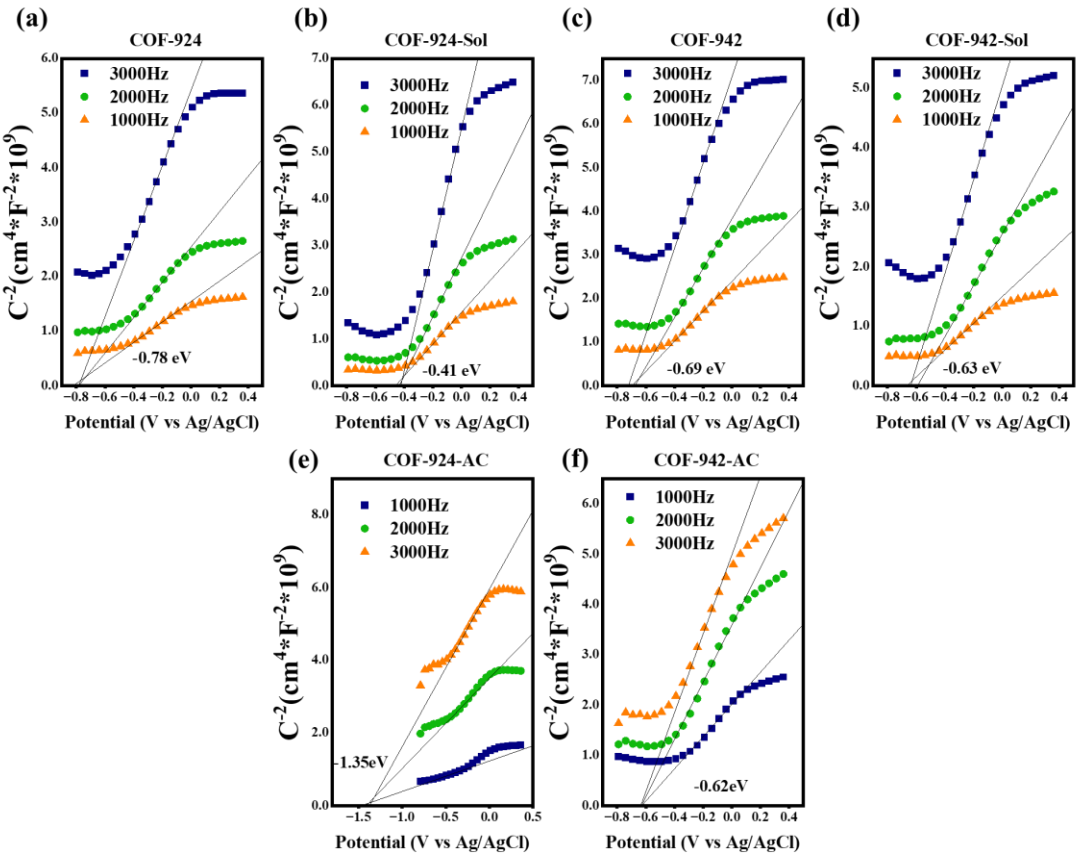

Figure S49. Mott–Schottky plots of all COFs: (a) COF-924, (b) COF-924-Sol, (c) COF-942, (d) COF-942-Sol, (e) COF-924-AC, (f) COF-942-AC.

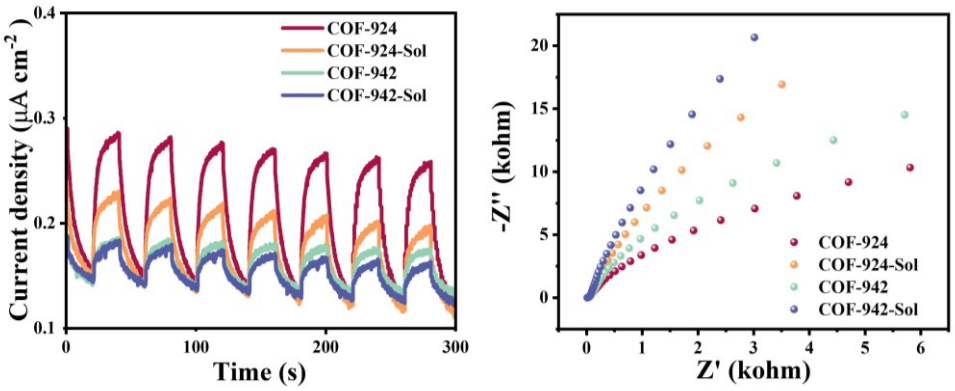

Figure S50. Transient photocurrent responses of COF-924 and COF-942 under irradiation with visible light and Electrochemical impedance spectroscopy of COF-924 and COF-942 with or without irradiation with visible light.

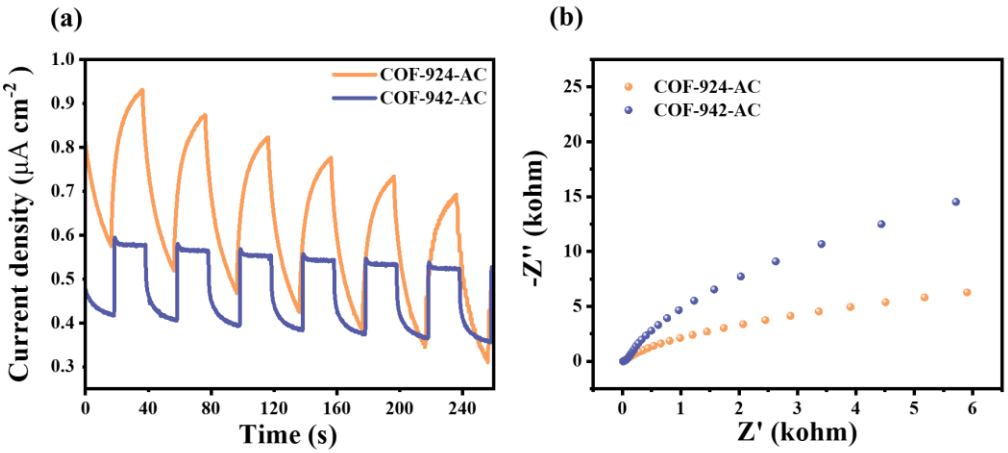

Figure S51. (a) Transient photocurrent responses of COF-924-AC and COF-942-AC under irradiation with visible light. (b) Electrochemical impedance spectroscopy (EIS) Nyquist plots of COF-924-AC and COF-942-AC.

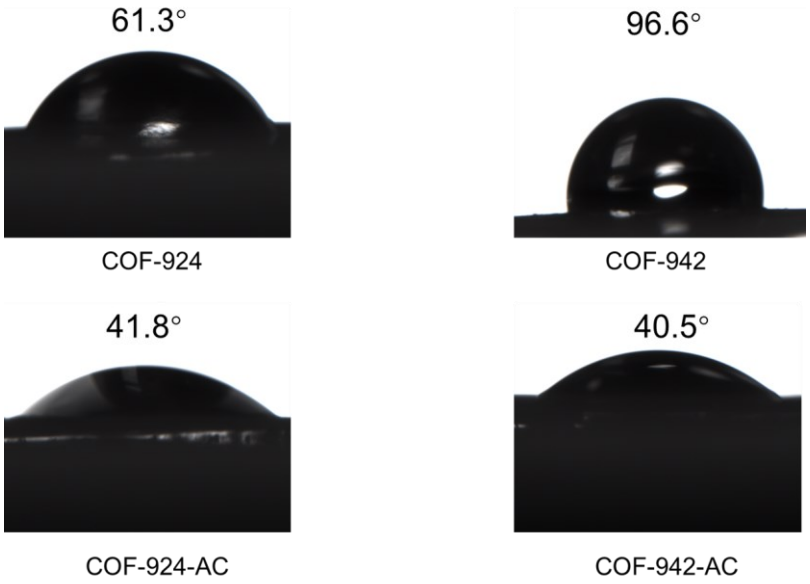

Figure S52. Water contact angle measurements for COF-924, COF-942, COF-924-AC, and COF-942-AC.

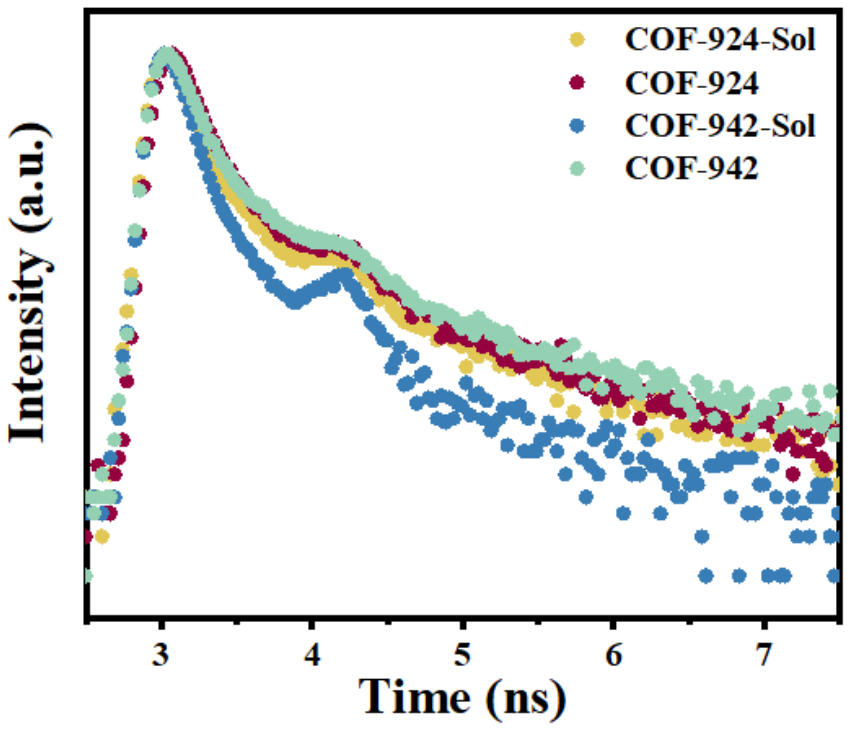

Figure S53. Time-resolved photoluminescence (TRPL) spectroscopy of COFs

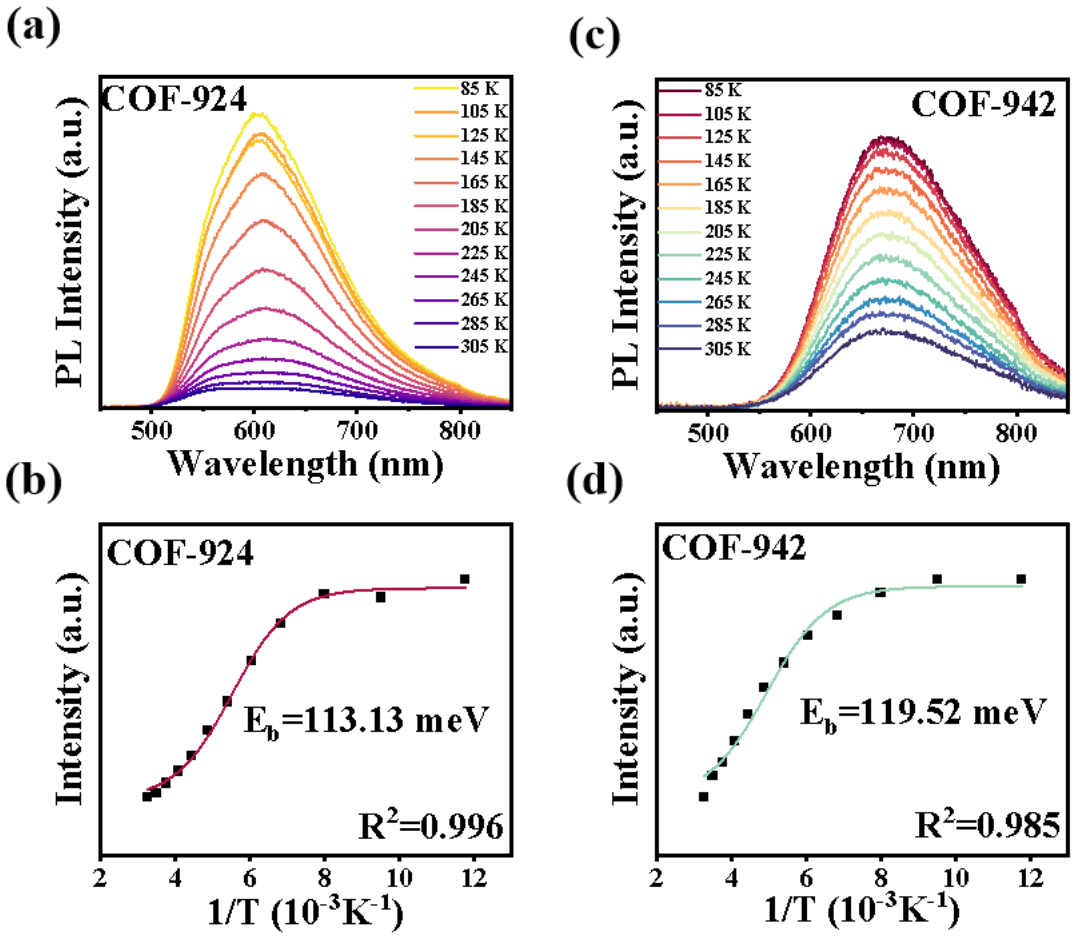

Figure S54. (a, c) Temperature-dependent photoluminescence (TD-PL) of COF-924 and COF-942; (b, d) Arrhenius plots used to extract exciton binding energies (E_b) of COF-924 and COF-942.

Section S7. Structural simulation

Molecular modeling of all COFs was generated with the Materials Studio (ver. 8.0) suite of programs. Pawley refinement was carried out using Reflex, a software package for crystal determination from PXRD pattern. Unit cell dimension was set to the theoretical parameters. The Pawley refinement was performed to optimize the lattice parameters iteratively until the R_{wp} value converges and the overlay observed with refined profiles shows good agreement. The lattice models (cell parameters, atomic positions, and total energy) were then fully optimized using Materials Studio Forcite

molecular dynamics module method. P1 space group was chosen for the primitive models in the initial simulations.

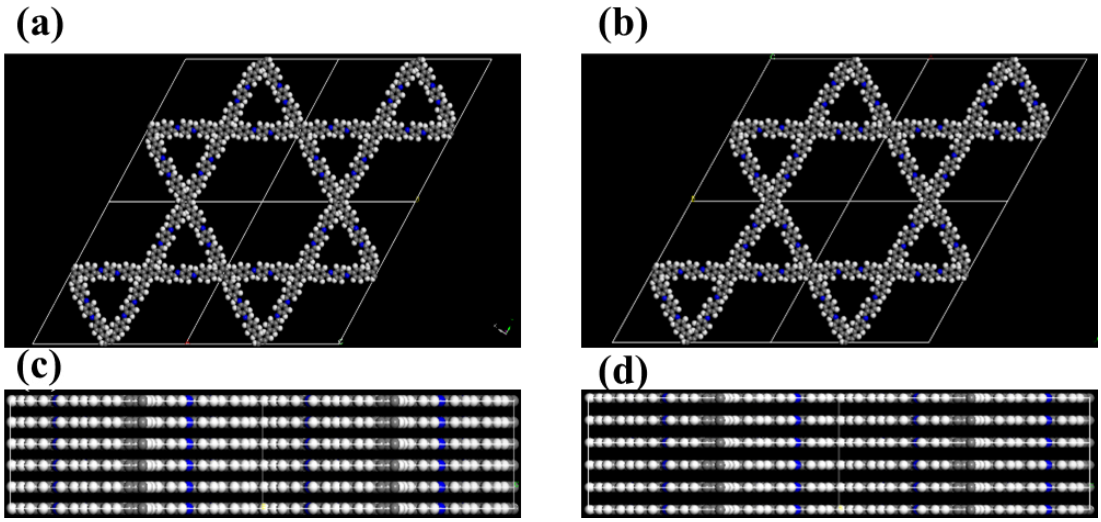

Figure S55. (a) and (c) top view and side view of **kgm** simulated AA stacking COF-924; (b) and (d) top view and side view of **kgm** simulated AA stacking COF-942.

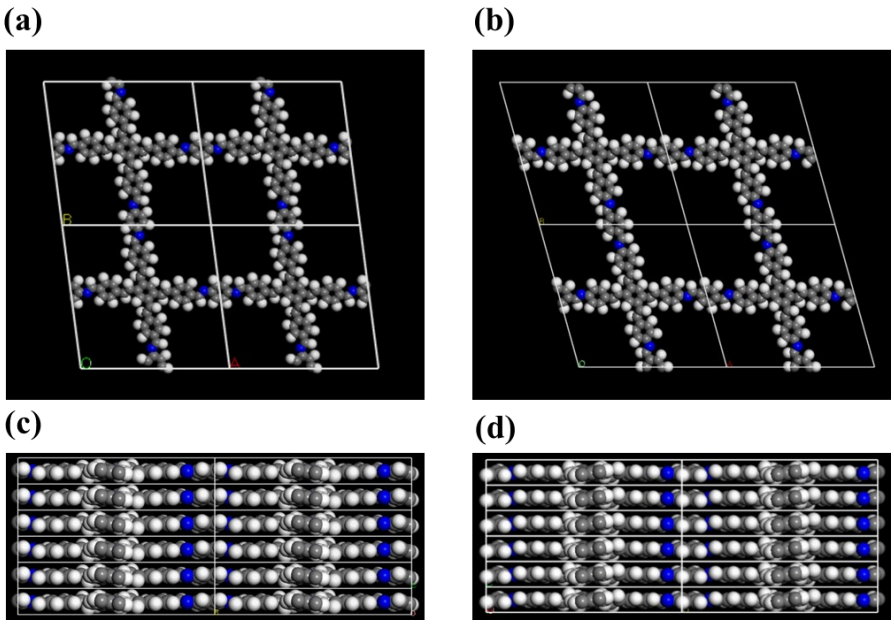

Figure S56. (a) and (c) top view and side view of **sql** simulated AA stacking COF-924; (b) and (d) top view and side view of **sql** simulated AA stacking COF-942.

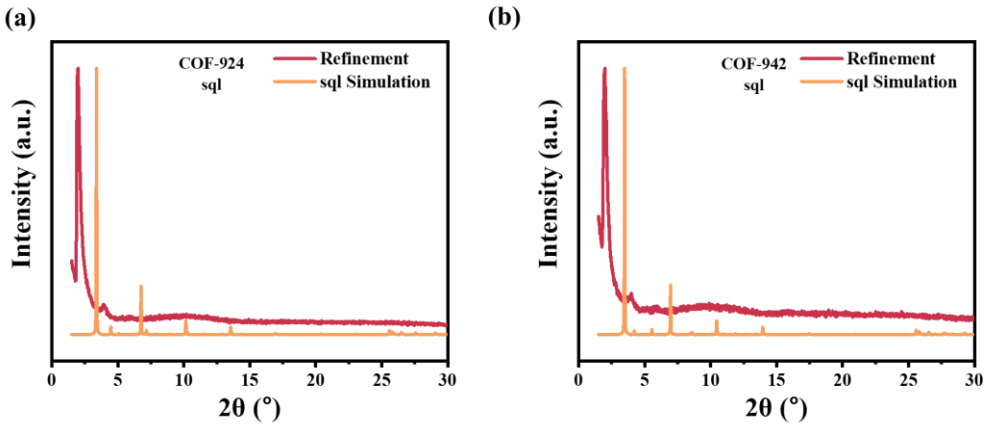

Figure S57. (a) Refined and simulated powder X-ray diffraction patterns of COF-924. (b) Refined and simulated powder X-ray diffraction patterns of COF-942.

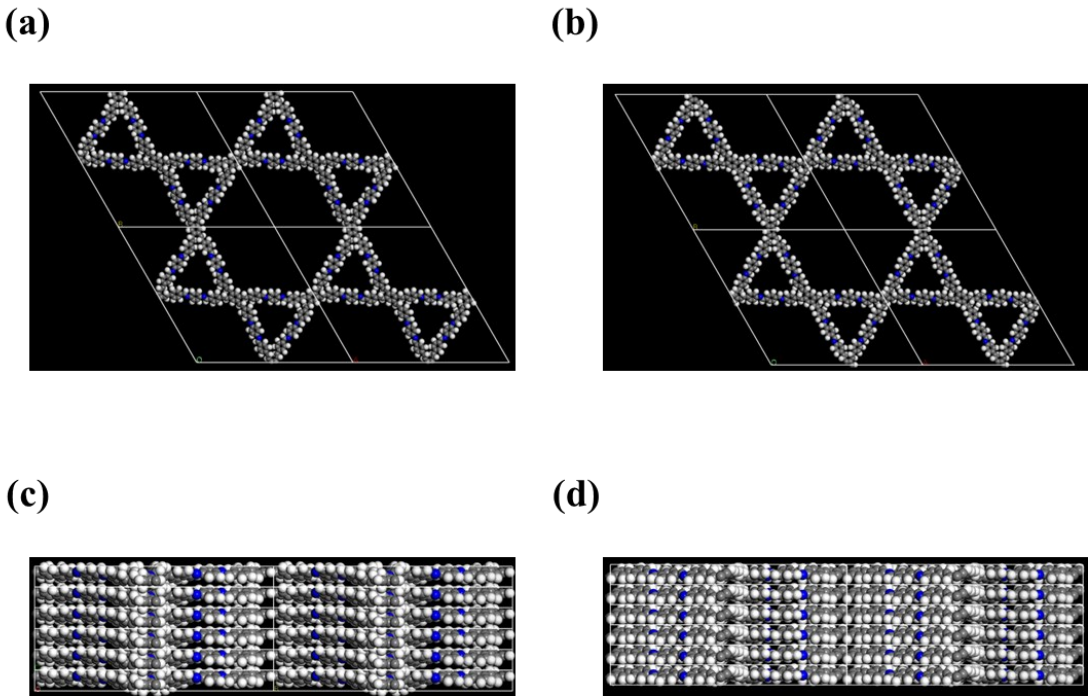

Figure S58. (a) and (c) top view and side view of **kgm (2)** simulated AA stacking COF-924; (b) and (d) top view and side view of **kgm (2)** simulated AA stacking COF-942.

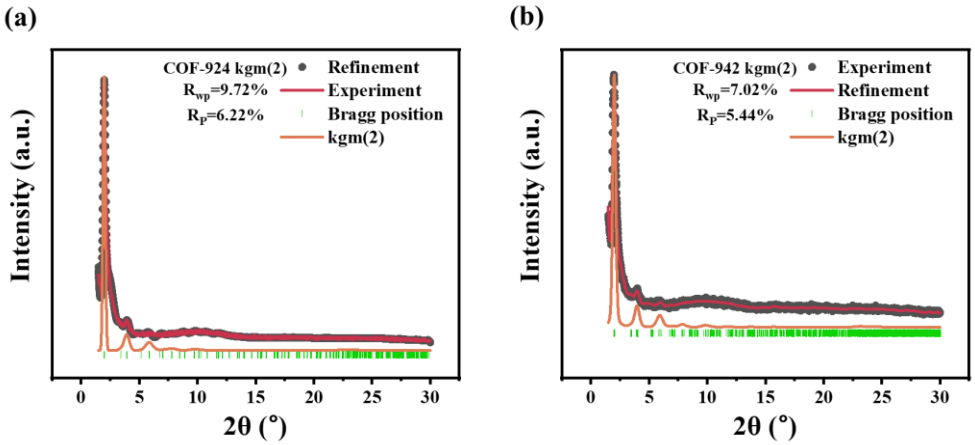

Figure S59. (a) Refined and **kgm (2)** simulated powder X-ray diffraction patterns of COF-924. (b) Refined and **kgm (2)** simulated powder X-ray diffraction patterns of COF-942.

Section S8. DFT calculations

DFT calculations were carried out using the B3LYP functional and the 6-311G (d, p) basis set as implemented in Gaussian09 program (Revision D. 01). The calculation of the excited state was performed using the time-dependent DFT (TDDFT) method at the level of B3LYP/6-31G*. Multiwfn is used for electronic orbitals analysis and electrostatic potential. A hole−electron analysis of COF-924 and COF-942 was performed in the Multiwfn 3.7(dev) program, and the hole delocalization index (HDI), the electron delocalization index (EDI) were calculated. Visualisation images of electronic orbitals were obtained from VMD software (version 1.9.3).[1, 2]

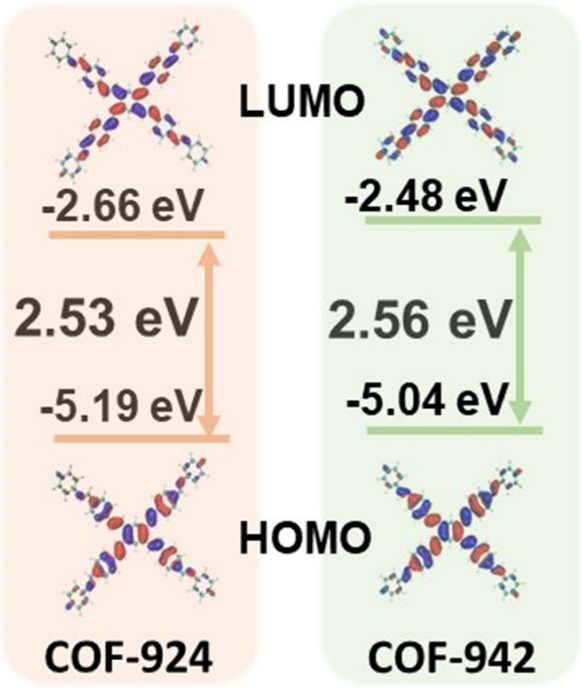

Figure S60. Calculated HOMO–LUMO gaps of COF-924,COF-942.

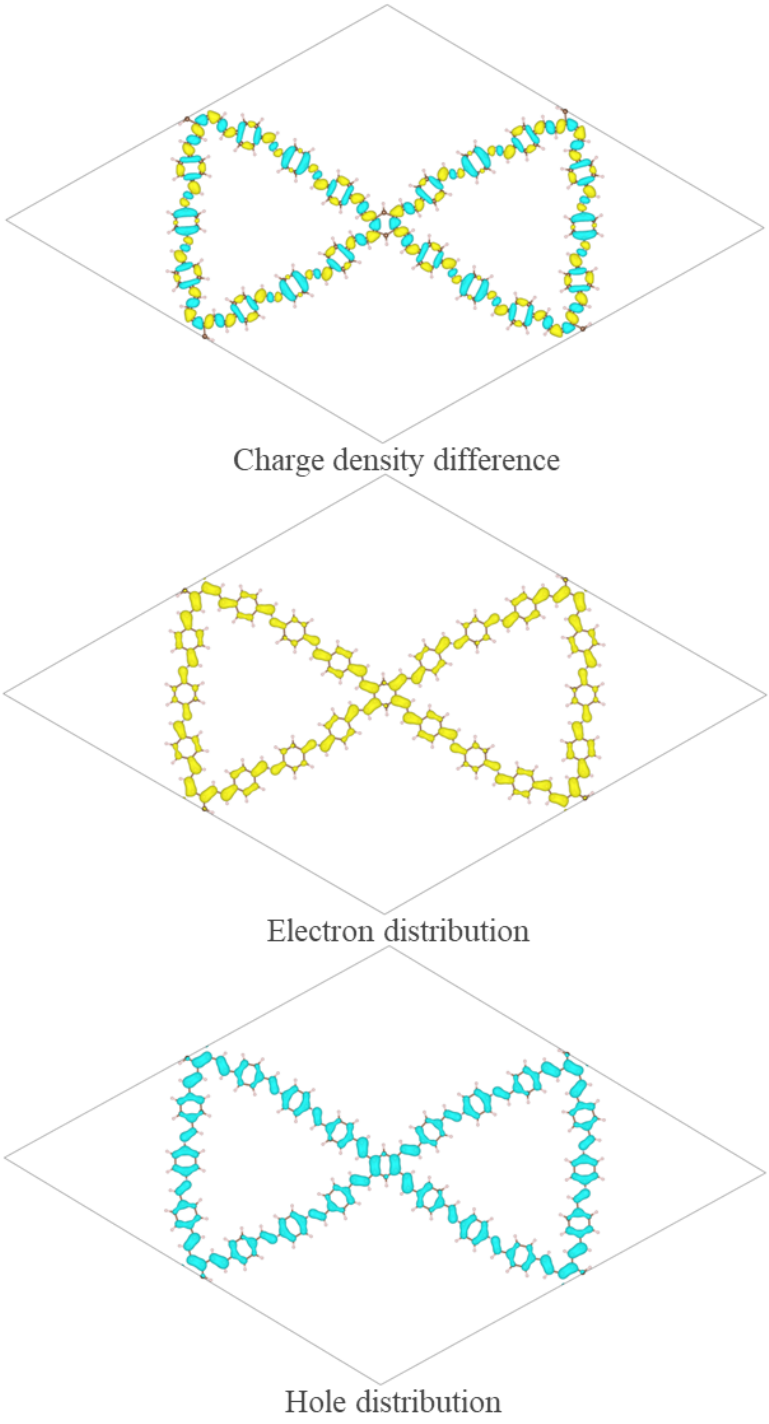

Figure S61. hole-electron analysis of COF-924.

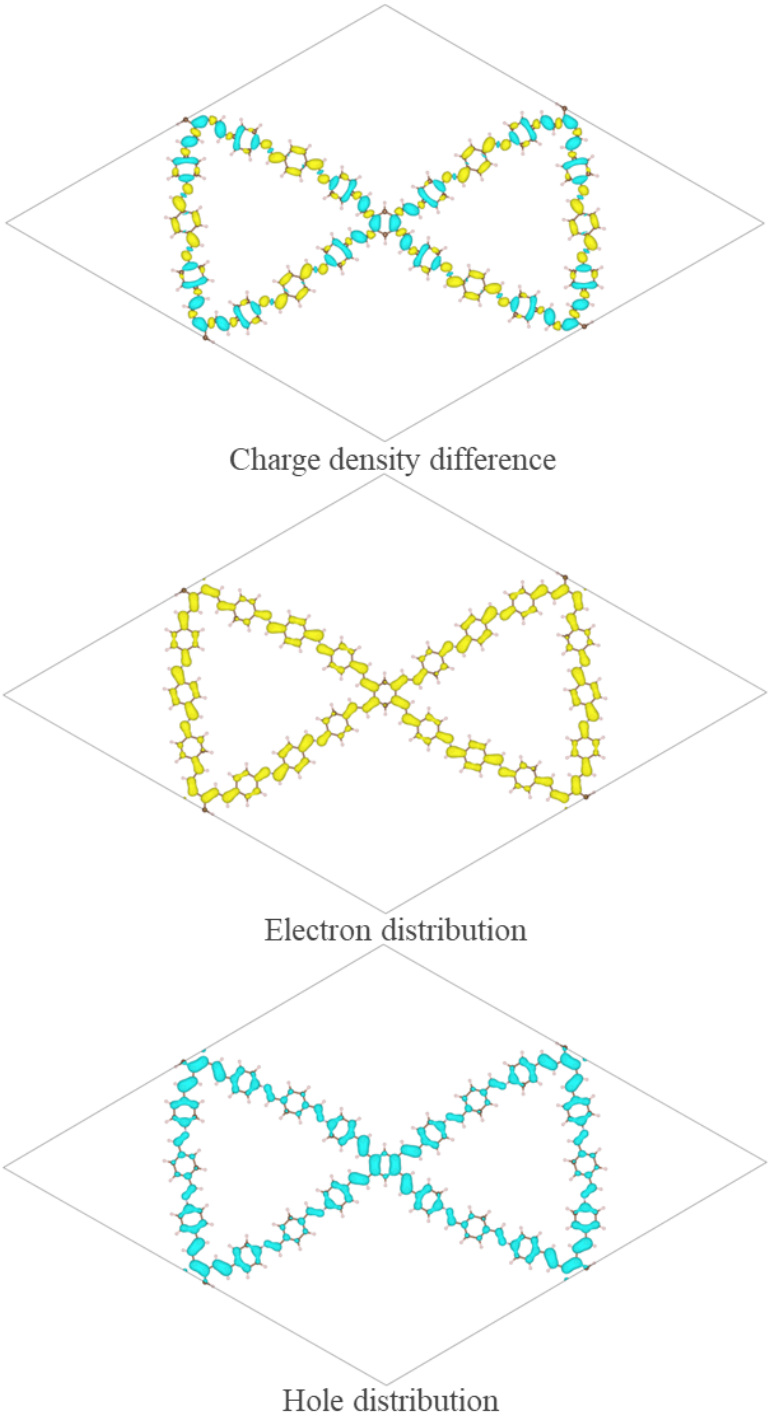

Figure S62. hole-electron analysis of COF-942.

Table S2. Critical reference parameters for electron-hole calculations.

S0→S1	D(Å)	S_r	S_m	H(Å)	t(Å)	E_{coul}(eV)	HDI	EDI
COF-924	0.003	0.86248	0.62789	18.858	-2.402	1.067491	2.13	2.18
COF-942	0.007	0.83975	0.56625	18.821	-11.794	1.067797	2.25	2.21

hole delocalization index (HDI) ,electron delocalization index (EDI).

$$HDI = 100 \times \sqrt{\int [\rho^{hole}(\boldsymbol{r})]^2 \mathrm{d}\boldsymbol{r}}$$

$$HDI = 100 \times \sqrt{\int [\rho^{ele}(\boldsymbol{r})]^2 \mathrm{d}\boldsymbol{r}}$$

Table S3. The photocatalytic hydrogen evolution performance comparison of COFs in this study with other COFs under visible light sunlight.

COFs	Light	Co-catalyst	Sacrificial agent	Activities ($\mu mol \cdot g^{-1} \cdot h^{-1}$)	ref.
COF-924	**420-780 nm**	**Pt**	**ascorbic acid**	**154800**	**This work**
HCl-COF-920	350-780 nm	Pt	ascorbic acid	364000	Angew. Chem. Int. Ed. 2025, e202511200
HCl-COF-920	420-780 nm	Pt	ascorbic acid	257000	Angew. Chem. Int. Ed. 2025, e202511200
COF-920	420-780 nm	Pt	ascorbic acid	22100	Angew. Chem. Int. Ed. 2025, e202511200
COF-JLU-45	> 420 nm	Pt	ascorbic acid	272500	Angew. Chem. Int. Ed. 2025, e202501869
IMDA-AA	> 420 nm	Pt	ascorbic acid	171200	Adv. Mater. 2025, 2500468
TpPa-SCOF-An	> 420 nm	Pt	ascorbic acid	126000	Nat. Commun. 2025, 16, 1940
CTC-COF-AB	> 420 nm	Pt	triethanolamine	113640	Appl. Catal. B Environ. 2025, 372, 125301
TpBP-CN COF	> 420 nm	Pt	ascorbic acid	162720	Chin. J. Chem. 2024, 42, 2621-2626
COF-954	> 420 nm	Pt	ascorbic acid	137226	Adv. Mater. 2024, 36, 2308251
PB-COF-Pt	> 400 nm	Pt	ascorbic acid	80400	ChemSusChem 2024, 17, e202400556
Q1DCOF-13	> 420 nm	Pt	ascorbic acid	79600	J. Am. Chem. Soc. 2024, 146, 26198–26206.
CH3I-TpPa-1	> 420 nm	none	ascorbic acid	9210	Nat. Commun. 2024, 15, 9576
COF-935	> 420 nm	Pt	ascorbic acid	67550	Angew. Chem.Int. Ed. 2023, 62, e202304611

COF-BBT	> 420 nm	Pt	ascorbic acid	48700	Natl. Sci. Rev. 2023, 10, nwac171
2D-TPs	> 420 nm	Pt	triethanolamine	26400	J. Am. Chem. Soc. 2023, 145, 12745–12754
BTz-COF-S	> 420 nm	Pt	ascorbic acid	19770	ACS Catal. 2023, 13, 15439−15447
CYANO-CON	> 420 nm	Pt	ascorbic acid	134200	Nat Commun. 2022 13, 2357
COF-JLU100	> 420 nm	Pt	triethanolamine	107308	Angew. Chem. Int. Ed. 2022, 61, e202208919
PY-DHBD-COF	> 420 nm	Pt	ascorbic acid	71160	Nat. Commun., 2022, 13, 1355
DCNA-1_AC	> 420 nm	Pt	ascorbic acid	27887	Nat. Commun. 2022, 13, 6317
sonoCOF-3	> 420 nm	Pt	ascorbic acid	16600	Nat. Synth. 2022, 1, 87-95
Pt1@TpPa-1	> 420 nm	Pt	sodium ascorbate	99860	ACS Catal. 2021, 11, 13266−13279
TtaTfa_AC	> 420 nm	Pt	ascorbic acid	20700	Angew. Chem. Int. Ed. 2021, 60, 2-9
30%PEG@BT-COF	> 420 nm	Pt	ascorbic acid	11140	Nat. Commun. 2021, 12, 3934
Py-ClTP-BT-COF	> 420 nm	Pt	ascorbic acid	8875	Angew. Chem. Int. Ed. 2020, 59, 16902-16909
g-$C_{18}N_3$-COF	> 420 nm	Pt	ascorbic acid	2920	Nat. Commun. 2019, 10, 2467

Table S4. Comparison of COF-924 with other imine-linked COFs.

COFs	Light	Co-catalyst	Sacrificial agent	Activities ($\mu mol \cdot g^{-1} \cdot h^{-1}$)	ref.
COF-924	420-780 nm	Pt	ascorbic acid	154800	This work
HCl-COF-920	420-780 nm	Pt	ascorbic acid	257000	Angew. Chem. Int. Ed. 2025, e202511200
COF-920	420-780 nm	Pt	ascorbic acid	22100	Angew. Chem. Int. Ed. 2025, e202511200
IMDA-AA	> 420 nm	Pt	ascorbic acid	171200	Adv. Mater. 2025, 2500468
CTC-COF-AB	> 420 nm	Pt	triethanolamine	113640	Appl. Catal. B Environ. 2025, 372, 125301
BMTB-BTTC-COF	> 420 nm	Pt	ascorbic acid	12370	Chin. J. Chem., 43: 1199-1207.
COF-BP-Ni2	420-780 nm	Pt	ascorbic acid	12210	Inorg. Chem. 2025, 64,4524−4533
PC-NPB	> 420 nm	Pt	ascorbic acid	15700	Sci China Chem, 2025, 68
COF-954	> 420 nm	Pt	ascorbic acid	137226	Adv. Mater. 2024, 36, 2308251
PB-COF-Pt	> 400 nm	Pt	ascorbic acid	80400	ChemSusChem 2024, 17, e202400556
Q1DCOF-13	> 420 nm	Pt	ascorbic acid	79600	J. Am. Chem. Soc. 2024, 146, 26198–26206.
CH3I-TpPa-1	> 420 nm	none	ascorbic acid	9210	Nat. Commun. 2024, 15, 9576
COF-935	> 420 nm	Pt	ascorbic acid	67550	Angew. Chem.Int. Ed. 2023, 62, e202304611
PY-DHBD-COF	> 420 nm	Pt	ascorbic acid	71160	Nat. Commun., 2022, 13, 1355
DCNA-1_AC	> 420 nm	Pt	ascorbic acid	27887	Nat. Commun. 2022, 13, 6317
sonoCOF-3	> 420 nm	Pt	ascorbic acid	16600	Nat. Synth. 2022, 1, 87-95
TtaTfa_AC	> 420 nm	Pt	ascorbic acid	20700	Angew. Chem. Int. Ed. 2021, 60, 2-9

Py-ClTP-BT-COF	> 420 nm	Pt	ascorbic acid	8875	Angew. Chem. Int. Ed. 2020, 59, 16902-16909

Table S5. Unit cell parameters and fractional atomic coordinates for COF-924 based on the AA-stacking.

Space group	P6/m (No. 175)		
Calculated unit cell	a = b = 51.9037 Å, c = 3.9613 Å α = β = 90°, γ = 120°		
Atom	x/a	y/b	z/c
C1	0.00298	0.48046	0
C2	0.02926	0.50852	0
C3	0.02635	0.53485	0
C4	0.04884	0.56625	0
C5	0.08031	0.58188	0
C6	0.09918	0.61321	0
C7	0.1301	0.62415	0
C8	0.15038	0.65446	0
C9	0.14067	0.67534	0
C10	0.10994	0.66488	0
C11	0.08936	0.63421	0
C12	0.16137	0.70592	0
C13	0.05694	0.50919	0
C14	0.06306	0.48548	0
C15	0.09223	0.4895	0
C16	0.11837	0.51779	0
C17	0.14638	0.52047	0
C18	0.14968	0.4953	0
C19	0.12404	0.46701	0
C20	0.0957	0.4642	0
C21	0.21329	0.769	0
C22	0.21489	0.74271	0
C23	0.24271	0.74475	0
C24	0.26873	0.77222	0
C25	0.2676	0.79886	0
C26	0.23955	0.79681	0

N27	0.29252	0.82638	0
N28	0.1908	0.71496	0
C29	3/6	0.32109	0
H30	0.00518	0.46098	0
H31	0.04012	0.58118	0
H32	0.09292	0.57116	0
H33	0.13895	0.60914	0
H34	0.17382	0.66135	0
H35	0.10177	0.68043	0
H36	0.06612	0.62773	0
H37	0.15372	0.72187	0
H38	0.07558	0.52947	0
H39	0.04523	0.46272	0
H40	0.11838	0.53853	0
H41	0.16571	0.54264	0
H42	0.12577	0.44706	0
H43	0.0764	0.44205	0
H44	0.19218	0.76839	0
H45	0.24426	0.72469	0
H46	0.28921	0.77172	0
H47	0.23802	0.81687	0
H48	0.52235	0.32587	0

Table S6. Unit cell parameters and fractional atomic coordinates for COF-942 based on the AA-stacking.

Space group	P6/m (No. 175)		
Calculated unit cell	a = b = 51.5123 Å, c = 4.3487 Å α = β = 90°, γ = 120°		
Atom	x/a	y/b	z/c
C1	1.24003	-0.48538	0
C2	1.21638	-0.51515	0
C3	1.22275	-0.53855	0
C4	1.18673	-0.5218	0
C5	1.00456	-0.52532	0
C6	1.03	-0.49663	0
C7	1.02616	-0.47113	0
C8	1.04934	-0.44116	0
C9	1.07978	-0.43168	0
C10	1.10234	-0.40187	0
C11	1.13206	-0.39555	0
C12	1.15554	-0.36592	0
C13	1.14956	-0.34211	0
C14	1.11978	-0.34848	0
C15	1.09625	-0.37819	0
N16	1.17195	-0.31313	0
C17	1.0584	-0.49375	0
C18	1.06403	-0.51748	0
C19	1.09304	-0.51287	0
C20	1.1182	-0.4839	0
C21	1.14707	-0.47987	0
C22	1.1513	-0.50463	0
C23	1.12616	-0.53367	0
C24	1.09722	-0.53769	0
C25	1.21777	-0.25164	0
C26	1.22397	-0.27525	0
C27	1.25371	-0.26886	0
C28	1.20132	-0.305	0
N29	1.17966	-3/6	0
H30	0.23421	0.53469	0

H31	0.20283	0.43803	0
H32	1/6	0.4547	0
H33	0.00636	0.45484	0
H34	0.04297	0.57854	0
H35	0.0867	0.55197	0
H36	0.13637	0.5862	0
H37	0.1789	0.63995	0
H38	0.11375	0.67145	0
H39	0.07118	0.61763	0
H40	0.07701	0.53117	0
H41	0.04372	0.45929	0
H42	0.11424	0.53737	0
H43	1/6	0.54457	0
H44	0.12848	0.4468	0
H45	0.07606	0.43957	0
H46	0.1927	0.74417	0
H47	0.25808	0.71294	0
H48	0.20632	0.67723	0

Reference

(1) Lu, T.; Chen, F. Multiwfn: A Multifunctional Wavefunction Analyzer. *J Comput Chem* **2012**, *33* (5), 580–592. https://doi.org/10.1002/jcc.22885.

(2) Liu, Z.; Lu, T.; Chen, Q. An Sp-Hybridized All-Carboatomic Ring, Cyclo[18]Carbon: Bonding Character, Electron Delocalization, and Aromaticity. *Carbon* **2020**, *165*, 468–475. https://doi.org/10.1016/j.carbon.2020.04.099.